Atmos. Chem. Phys., 21, 16093–16120, 2021
https://doi.org/10.5194/acp-21-16093-2021

Atmospheric Chemistry and Physics
Open Access

Influence of atmospheric in-cloud aqueous-phase chemistry on the global simulation of SO_2 in CESM2

Wendong Ge[1], Junfeng Liu[1], Kan Yi[2], Jiayu Xu[1], Yizhou Zhang[1], Xiurong Hu[3], Jianmin Ma[1], Xuejun Wang[1], Yi Wan[1], Jianying Hu[1], Zhaobin Zhang[1], Xilong Wang[1], and Shu Tao[1]

[1]Laboratory for Earth Surface Processes, College of Urban and Environmental Sciences, Peking University, Beijing 100871, China
[2]Institute of Science and Technology, China Three Gorges Corporation, Beijing 100038, China
[3]College of Economics and Management, Nanjing University of Aeronautics and Astronautics, Nanjing 211106, China

Correspondence: Junfeng Liu (jfliu@pku.edu.cn)

Received: 14 May 2021 – Discussion started: 16 June 2021
Revised: 3 September 2021 – Accepted: 4 October 2021 – Published: 2 November 2021

Abstract. Sulfur dioxide (SO_2) is a major atmospheric pollutant and precursor of sulfate aerosols, which influences air quality, cloud microphysics, and climate. Therefore, better understanding the conversion of SO_2 to sulfate is essential to simulate and predict sulfur compounds more accurately. This study evaluates the effects of in-cloud aqueous-phase chemistry on SO_2 oxidation in the Community Earth System Model version 2 (CESM2). We replaced the default parameterized SO_2 aqueous-phase reactions with detailed HO_x, Fe, N, and carbonate chemistry in cloud droplets and performed a global simulation for 2014–2015. Compared with the observations, the results incorporating detailed cloud aqueous-phase chemistry greatly reduced SO_2 overestimation. This overestimation was reduced by 0.1–10 ppbv (parts per billion by volume) in most of Europe, North America, and Asia and more than 10 ppbv in parts of China. The biases in annual simulated SO_2 mixing ratios decreased by 46 %, 41 %, and 22 % in Europe, the USA, and China, respectively. Fe chemistry and HO_x chemistry contributed more to SO_2 oxidation than N chemistry. Higher concentrations of soluble Fe and higher pH values could further enhance the oxidation capacity. This study emphasizes the importance of detailed in-cloud aqueous-phase chemistry for the oxidation of SO_2. These mechanisms can improve SO_2 simulation in CESM2 and deepen understanding of SO_2 oxidation and sulfate formation.

1 Introduction

Sulfur dioxide (SO_2) is one of the major atmospheric pollutants. The anthropogenic emission of SO_2 is the greatest source, which includes mainly the combustion of fossil fuel in the power and steel industries (Buchard et al., 2014). Human health risks from SO_2 have also been discovered and discussed in many studies (Kan et al., 2012; Tong et al., 2017; Chen et al., 2018). More importantly, SO_2 is the precursor of sulfate aerosols. Sulfate can be regarded as one of the core species in the atmosphere. First, it is one of the major components of fine particles ($PM_{2.5}$) which cause haze pollution and affect human health, especially in East and South Asia (Buchard et al., 2014; Chen et al., 2018; Quan et al., 2015; Geng et al., 2019). In addition, sulfate is also the main component of cloud condensation nuclei (CCN), which directly influences the formation of clouds and, thus, affects precipitation, solar radiation, and climate (He et al., 2015a; Tang et al., 2016). Moreover, sulfate itself is also one of the key species affecting radiative forcing, which directly influences climate change (J. Li et al., 2018; Pöschl and Shiraiwa, 2015; Xie et al., 2016). Therefore, only through a better understanding of SO_2, especially the process of its oxidation to sulfate, can we better understand sulfate and explore all the issues above (Hung et al., 2018).

SO_2 can be oxidized to sulfate in multiple ways. On clear and sunny days, the gas-phase oxidation of SO_2 by OH radicals (•OH) is the dominant pathway (J. Li et al., 2018; Cheng et al., 2016). However, when relative humidity (RH) and

$PM_{2.5}$ increase on cloudy, foggy, or hazy days, solar radiation and photochemical reactions decrease dramatically, resulting in a sharp decrease in gaseous •OH and, thus, the gas-phase oxidation of SO_2, especially in winter. Alternatively, the aqueous-phase oxidation of SO_2 becomes much more important because of the increase in atmospheric liquid water content (Cheng et al., 2016; Quan et al., 2015). Aqueous-phase chemistry is an important part of atmospheric chemistry. Various physical and chemical parameters, such as the water content, ionic strength, and pH value, could directly affect the gas–aqueous mass transfer process and the reaction rates and then influence the relative contributions of various mechanisms (Elser et al., 2016; Ervens, 2015). For SO_2, the aqueous-phase oxidation of SO_2 by diverse oxidants can serve as the major sink of atmospheric SO_2. It accounts for nearly 80 % of global sulfate production, and more than half of sulfate production occurs in clouds (Harris et al., 2013; Huang et al., 2018). Specifically, there are several common oxidation pathways in the aqueous phase, such as oxidation by hydrogen peroxide (H_2O_2) and ozone (O_3; Tan et al., 2016; Hung et al., 2018). In recent years, increasing numbers of studies have focused on the catalytic effect of transition metal ions (TMIs) on the aqueous-phase oxidation of SO_2 (Tilgner et al., 2013; Alexander et al., 2009). In addition, oxidation by NO_2 has also received increasing attention (Xue et al., 2016).

Transition metals in dust particles are important sites for various reactions and affect the moisture absorption, light scattering, and nucleation process of clouds. Among these elements, Fe is one of the most important transition metals due to its high abundance and activity (Tang et al., 2016). Soluble Fe can act as an important catalyst in the Fenton reaction for the oxidation of SO_2 when dissolved into the aqueous phase. The Fenton reaction, which was first proposed by Henry J. H. Fenton in the 1890s, is one of the most important and widespread reactions in multiphase chemistry (Wiegand et al., 2017; Fenton, 1894; Pöschl and Shiraiwa, 2015). This reaction involves the production of •OH in the aqueous phase by the decomposition of H_2O_2 catalyzed by low-valence TMIs such as Fe^{2+} (Deguillaume et al., 2005; Herrmann et al., 2015). Different mechanisms have been developed to explain the first step of Fenton reactions. Of the best known pathways, two are (1) the OH radical mechanism ($Fe^{2+} + H_2O_2 \rightarrow Fe^{3+} + \bullet OH + OH^-$) developed by Haber and Weiss (1934) and (2) the non-OH radical mechanism ($Fe^{2+} + H_2O_2 \rightarrow FeO^{2+} + H_2O$) proposed by Bray and Gorin (Haber and Weiss, 1934; Bray and Gorin, 1932; Wiegand et al., 2017; Pöschl and Shiraiwa, 2015). The relative contributions of these two pathways differ under various conditions and remain controversial. A recent experimental study suggested that the non-OH radical mechanism is dominant under nearly neutral conditions (pH $\approx$ 7), while the OH radical mechanism becomes more important under acidic conditions (Pang et al., 2011; Deguillaume et al., 2005; Wiegand et al., 2017; Pöschl and Shiraiwa, 2015; Bataineh et al., 2012). Then, all of these oxidative intermediates (i.e., Fe^{3+}, •OH, and FeO^{2+}) can further oxidize SO_2 to sulfate. In this way, Fe^{3+} and FeO^{2+} are reduced to Fe^{2+}, thus forming a complete redox cycle. Their concentrations and proportions are basically the same during the redox cycle, and a balance of catalysts is achieved (Deguillaume et al., 2005). The effects of soluble Fe on sulfate formation have been discussed in several studies (Gankanda et al., 2016). In addition, direct oxidation of SO_2 by O_2 might also be catalyzed by soluble Fe. In general, Fenton reactions could lead to faster radical recycling. The reaction rates of sulfate formation are enhanced with high Fe concentrations, especially when pH < 5 (Shao et al., 2019; Ervens, 2015; Huang et al., 2014; Tilgner et al., 2013).

On the other hand, a number of studies have also emphasized the important role of NO_2 in the oxidation of SO_2 (Ma et al., 2018; Tao et al., 2017; Huang et al., 2019). He et al. (2014) and Cheng et al. (2016) reported a missing source of SO_2 oxidation that can be explained by the synergistic effect between NO_2 and SO_2 in aerosol water and on mineral dust as follows: $2NO_2 + HSO_3^- + H_2O \rightarrow 3H^+ + 2NO_2^- + SO_4^{2-}$ (He et al., 2014; Cheng et al., 2016). Such a conversion of SO_2 by NO_2 is driven by a high pH value (e.g., pH > 5.5) and a high concentration of NO_2 (Wang et al., 2020; L. Li et al., 2018; Huang et al., 2019; He and He, 2020; He et al., 2018). Moreover, these studies have indicated that > 95 % of NO_2 converts to HNO_2/NO_2^- by hitting the surface of $NaHSO_3$ aqueous microjets to promote the aqueous-phase oxidation of SO_2 (Wang et al., 2020; L. Li et al., 2018). This pathway can explain the gaps in sulfate concentrations between simulations and observations from approximately 15 % to 65 % during haze days in winter (Zheng et al., 2020). However, other studies have suggested that the contribution of nitrogen chemistry to SO_2 oxidation is very limited. Au Yang et al. (2018) argued that the NO_2 oxidation pathway cannot explain the extreme concentrations of sulfate measured in urban aerosols (Au Yang et al., 2018). Only a minor (approximately 2 %) fraction of heterogeneous sulfate formation occurs via the oxidation of SO_2 by NO_2 (Shao et al., 2019). The main reason is that the pH value is hardly ever high enough to maintain the efficiency of oxidation by NO_2 in aerosol or cloud water (Guo et al., 2017). For instance, aerosols collected from several urban areas in China (CN) were always acidic (even with the unusually high NH_3 emissions and concentrations in northern CN), suggesting that oxidation by NO_2 might not be very important in these regions (Li et al., 2020; He and He, 2020). In summary, the contribution of N chemistry to the aqueous-phase oxidation of SO_2 still needs further investigation.

Many studies have been conducted on the aqueous-phase oxidation of SO_2. Some laboratory studies have focused on the detailed mechanism, such as the radical processes involved in different pathways of the Fenton reaction (Wiegand et al., 2017; Bataineh et al., 2012) and the conversion of NO_2 to HNO_2 to oxidize SO_2 (He et al., 2014). Some studies

have paid more attention to the measurement and updating of kinetic parameters (Cwiertny et al., 2008; He et al., 2018; He and He, 2020). More importantly, modeling studies have made great progress in revealing the mechanism of SO_2 oxidation and sulfate formation in the aqueous phase (Bell et al., 2005). For instance, Herrmann et al. (2000) used a box model to investigate the detailed aqueous-phase radical mechanism for tropospheric chemistry (Herrmann et al., 2000). Huang et al. (2014) and Li et al. (2017) discussed the enhancement of sulfate formation by mineral aerosols in CN and improved the simulation of heterogeneous sulfate in the Weather Research and Forecasting (WRF)-Chem model (Huang et al., 2014; Li et al., 2017). J. Li et al. (2018) also improved the simulation of sulfate with the nested air-quality prediction modeling system (NAQPMS) model of oxidation of SO_2 by NO_2 on wet aerosols on haze days (J. Li et al., 2018). Shao et al. (2019) evaluated various heterogeneous mechanisms for sulfate aerosol formation in Beijing using the GEOS-Chem model (Shao et al., 2019). Bell et al. (2005) analyzed the effects of different SO_2 emission scenarios on radiative forcing and climate over East Asia (EA) using the Global Climate Model (GCM; Bell et al., 2005). Both Zheng et al. (2020) and Zheng et al. (2015) used the Community Multiscale Air Quality (CMAQ) model to explore heterogeneous chemistry for the formation of secondary inorganic aerosols and the contribution of nitrate photolysis to heterogeneous sulfate formation in CN on winter haze days, respectively (Zheng et al., 2020; Zheng et al., 2015). Zheng et al. (2015) used the WRF-CMAQ model to explain the crucial role of reactive N chemistry in aerosol water for sulfate formation during haze events in CN (Zheng et al., 2015). Nevertheless, there are still obvious shortcomings in these model studies. First of all, in long-term global climate simulations, studies focused on the spatiotemporal distribution of SO_2 concentrations are still insufficient. Most studies have evaluated only sulfate distribution and its climate impact. Very few studies have discussed the simulation of SO_2, and these few studies are only from the perspective of SO_2 emissions. In addition, although some studies have attempted to discuss different pathways of aqueous-phase oxidation of SO_2, most of them have merely adopted simplified mechanisms or even parameterization alone without introducing detailed radical mechanisms. On the other hand, several studies investigated the detailed aqueous-phase chemistry, but they did not analyze its influence on SO_2 but only discussed the influence on O_3, •OH, or HO_2 (Herrmann et al., 2000; Jacob, 1986; Matthijsen et al., 1995; Jacob, 2000; Mao et al., 2013, 2017). Finally, the simulations of SO_2 in many studies are still highly overestimated (He et al., 2015b, a; Buchard et al., 2014; Hong et al., 2017; Georgiou et al., 2018; Wei et al., 2019; Flemming et al., 2015; Sha et al., 2019; X. Liu et al., 2012; Hedegaard et al., 2008), while others underestimate the concentration of sulfate (Xie et al., 2016; Goto et al., 2015; Bell et al., 2005; Lamarque et al., 2012; Pozzer et al., 2012; Guth et al., 2016; Wei et al., 2019; Geng et al., 2019; Kajino et al., 2012; Mathur, 2005; X. Liu et al., 2012; Sha et al., 2019; Zhang et al., 2012; Itahashi, 2018). All of these disadvantages indicate that the mechanism of SO_2 oxidation to sulfate is still not fully understood.

This study aims to examine the role played by detailed in-cloud aqueous-phase chemistry (not including chemical reactions on the surfaces of wet aerosols) on the capacity for oxidation of global SO_2 in the Community Earth System Model 2 (CESM2). We describe the CESM2 model, detailed cloud chemistry, and observational data in Sect. 2. The evaluation of SO_2 simulations with or without coupling detailed in-cloud aqueous-phase chemistry is given in Sect. 3. The contributions of different in-cloud aqueous-phase chemical mechanisms to the simulation of SO_2 are analyzed in Sect. 4. The key factors that affect the capacity for SO_2 oxidation are discussed in Sect. 5. Finally, the main conclusions are drawn in Sect. 6.

2 Methodology

2.1 Model description

The Community Earth System Model 2 (CESM2, v2.1.1), developed by the National Center for Atmospheric Research (NCAR; https://www.cesm.ucar.edu/models/cesm2/, last access: 16 December 2020), is used in this study (Emmons et al., 2020; Danabasoglu et al., 2020), configured with the Community Atmosphere Model version 4.0 (CAM4). The coupled chemistry in CAM4 is primarily based on the Model for Ozone and Related chemical Tracers, version 4 (MOZART-4), including 85 gas-phase species with bulk aerosols and detailed tropospheric chemistry with 196 gas-phase reactions (Emmons et al., 2010; Lamarque et al., 2012). The default aerosol species simulated in this component set include sulfate, nitrate, ammonium, black carbon (BC), organic carbon (OC), secondary organic aerosol (SOA), dust, and sea salt. In this study, we develop a detailed aqueous-phase chemistry module for SO_2 oxidation fully coupled in the MOZART-4 chemistry.

The model is configured with a horizontal resolution of 0.95° (latitude) × 1.25° (longitude) and 30 levels in the vertical direction from 993 (near-surface layer) to 3.6 hPa. The model is nudged by assimilated meteorological offline data from Modern-Era Retrospective analysis for Research and Applications, version 2 (MERRA-2, https://rda.ucar.edu/datasets/ds313.3/, last access: 20 July 2020), prepared with 14 meteorological variables (e.g., air temperature, surface pressure, specific humidity, and eastward and northward winds) to run CESM2 simulations. The meteorological data have a temporal resolution of 3 h.

All the emission inventories needed for MOZART-4 chemistry are obtained from the CESM database (https://svn-ccsm-inputdata.cgd.ucar.edu/trunk/inputdata/atm/cam/chem/emis/CMIP6_emissions_1750_2015/, last

access: 31 December 2020), which was developed for the Coupled Model Intercomparison Project (CMIP)6 projects (Feng et al., 2020). The inventories have been updated to 2015, which is the year of the simulation in this study. Meanwhile, the emission, dry deposition, and wet deposition processes of aerosol species are also guided by input files from CESM database (https://svn-ccsm-inputdata.cgd.ucar.edu/trunk/inputdata/atm/cam/chem/trop_mozart_aero/, last access: 31 December 2020; https://svn-ccsm-inputdata.cgd.ucar.edu/trunk/inputdata/atm/cam/chem/emis/CMIP6_emissions_1750_2015_2deg/, last access: 31 December 2020) and the source codes of CESM2 (aero_model.F90, mo_drydep.F90, and wetdep.F90).

The variables related to the cloud properties used in this study are all from the Rasch and Kristjansson (RK) prognostic cloud microphysical processes. These variables include the liquid water content of clouds (LWC; liters of water per liter of air; hereafter $L_{water} L_{air}^{-1}$), volume fraction of clouds (F_{cld}), and radius of cloud droplets (r; microns; hereafter µm). They are directly obtained from the model simulation and directly or indirectly influence the in-cloud aqueous-phase chemistry. Among these variables, the simulated r ranges from 8 to 14 µm, consistent with those in previous studies (Herrmann et al., 2000, 2015; Jacob, 1986; Matthijsen et al., 1995; J. Liu et al., 2012). Meanwhile, CESM2 simulates both large-scale stratiform clouds and convective clouds (i.e., shallow cumulus clouds and deep convective clouds). For each type of cloud, both water and ice are simulated. However, the SO_2 produced in convective clouds is assumed to be removed rapidly by convective precipitation. Thus, the contribution of SO_2 from shallow cumulus clouds and deep convective clouds is ignored. Only the LWC and F_{cld} of large-scale liquid stratiform clouds are employed in this study.

2.2 Mechanism of in-cloud aqueous-phase oxidation of SO_2

The detailed mechanism of in-cloud aqueous-phase oxidation of SO_2 is divided into the gas–aqueous-phase transfer process and aqueous-phase chemical mechanisms, as listed in Tables 1 and 2, respectively (see below). There are 32 (16 pairs of) gas–aqueous-phase transfer equilibria and 187 aqueous-phase reactions (only in cloud droplets and not on surfaces of wet aerosol), involving 46 new aqueous species in all. Specifically, the aqueous-phase reactions include 26 (13 pairs of) ionization equilibria and four different chemistry modules, which are HO_x chemistry, Fe chemistry, N chemistry, and carbonate chemistry. The aqueous-phase oxidation of SO_2 by H_2O_2 and O_3 is included in the HO_x chemistry mechanism. The two pathways of the Fenton reaction are included in the Fe chemistry mechanism. The aqueous-phase oxidation of SO_2 by NO_2 is included in the N chemistry mechanism.

There are four parameters in every pair of gas–aqueous-phase transfer equilibria. The two parameters in the transfer from the gas phase to the aqueous phase are the molar mass (grams per mole; hereafter $g\,mol^{-1}$) and mass accommodation coefficients of this species. The other two parameters in the transfer from the aqueous phase to the gas phase are Henry's law constants (moles per liter per atmosphere; hereafter $M\,atm^{-1}$) at 298 K (K_{H298}) and ΔH (joules per mole; hereafter $J\,mol^{-1}$)/R (joules per mole per Kelvin; hereafter $J\,mol^{-1}\,K^{-1}$), where ΔH is the enthalpy of dissolution. The Henry's law constant K_H ($M\,atm^{-1}$) at any temperature T (Kelvin; hereafter K) in Eq. (1) can be calculated by Eq. (2) as follows:

$$[C_i] = K_H \cdot P_i \tag{1}$$

$$K_H(T) = K_{H298} \cdot \exp\left(-\frac{\Delta H}{R}\left(\frac{1}{T} - \frac{1}{298}\right)\right), \tag{2}$$

where $[C_i]$ and P_i are aqueous-phase and gas-phase concentrations of species i in units of moles per liter of water (hereafter $mol\,L_{water}^{-1}$) and atmosphere, respectively. On the other hand, the concentration of liquid water is a constant value of 55.6 (i.e., 1000/18) $mol\,L^{-1}$. The initial concentration of soluble Fe(III) ($[Fe^{3+}]$) is set to 5 µM, which refers to the urban conditions from the literature (Deguillaume et al., 2005; Mao et al., 2013; Jacob, 2000; Shao et al., 2019; Li et al., 2017; Herrmann et al., 2000; Matthijsen et al., 1995).

To facilitate the calculation of gas-phase and aqueous-phase chemistry simultaneously, the methods used in Jacob (1986) and J. Liu et al. (2012) are applied in this study, which convert the units of concentrations and reaction rates in the aqueous phase to the same units as those used in gas-phase chemistry, as follows (Jacob, 1986; J. Liu et al., 2012):

$$[X_i] = 6.023 \times 10^{20} \cdot \mathrm{LWC} \cdot [C_i], \tag{3}$$

where $[X_i]$ and $[C_i]$ are aqueous-phase concentrations of species i in units of molecules per cubic meter of air (hereafter $molec.\,cm_{air}^{-3}$) and moles per liter of water (hereafter $mol\,L_{water}^{-1}$), respectively, and 6.023×10^{20} is the product of Avogadro constant (6.023×10^{23}) and unit conversion factor (10^{-3}) between values per liter of air (hereafter L_{air}^{-1}) and per cubic centimeter of air (hereafter cm_{air}^{-3}). In this way, the chemical systems of both gas and aqueous phases can be numerically solved without distinction.

2.3 Model configuration

There are two main simulations conducted in this study. The first simulation (the *original* case) is conducted without any modification of the default CAM4 chemistry, with parameterized aqueous-phase oxidation reactions of SO_2 by H_2O_2 and O_3. In the second simulation (the *improved* case), since the F_{cld} is nonzero in most grids, two calculations are performed in a cloudy grid cell. In the cloudy part, the parameterized aqueous-phase reactions mentioned above are replaced by detailed in-cloud aqueous-phase chemistry, listed

Table 1. Gas–aqueous-phase transfer equilibria. **(b)** Aqueous-phase chemistry.

No.	Reactions	k_1	k_2	Reference
	Gas–aqueous-phase transfer			
1[a, c]	$O_3(g) \rightarrow O_3$	48	0.05	Mirabel (1996)
2[b]	$O_3 \rightarrow O_3(g)$	1.1×10^{-2}	−2397	Hoffman and Calvert (1985); Pandis and Seinfeld (1989)
3[a]	$HO_2(g) \rightarrow HO_2$	33	0.01	Hanson et al. (1992)
4[b]	$HO_2 \rightarrow HO_2(g)$	9.0×10^3	0	Weinsteinlloyd and Schwartz (1991)
5[a]	$OH(g) \rightarrow OH$	17	0.05	Herrmann et al. (2000)
6[b]	$OH \rightarrow OH(g)$	25	−5280	Kläning et al. (1985)
7[a]	$H_2O_2(g) \rightarrow H_2O_2$	34	0.23	Seinfeld and Pandis (2016)
8[b]	$H_2O_2 \rightarrow H_2O_2(g)$	1.02×10^5	−6339	Lind and Kok (1994)
9[a]	$SO_2(g) \rightarrow SO_2$	64	$[1+\exp(14.7-3825/T)]^{-1}$	Boniface et al. (2000)
10[b]	$SO_2 \rightarrow SO_2(g)$	1.2	−3157	Olson and Hoffmann (1989)
11[a]	$CO_2(g) \rightarrow CO_2$	44	2×10^{-4}	Herrmann et al. (2000)
12[b]	$CO_2 \rightarrow CO_2(g)$	3.11×10^{-2}	−2422	Chameides (1984)
13[a]	$NH_3(g) \rightarrow NH_3$	17	0.04	Bongartz et al. (1995)
14[b]	$NH_3 \rightarrow NH_3(g)$	60.7	−3921	Clegg and Brimblecombe (1990)
15[a]	$HNO_3(g) \rightarrow HNO_3$	63	0.054	Davidovits et al. (1995)
16[b]	$HNO_3 \rightarrow HNO_3(g)$	2.1×10^5	−8696	Lelieveld and Crutzen (1991)
17[a]	$HCOOH(g) \rightarrow HCOOH$	46	0.012	Davidovits et al. (1995)
18[b]	$HCOOH \rightarrow HCOOH(g)$	5.53×10^3	−5629	Khan and Brimblecombe (1992)
19[a]	$CH_3COOH(g) \rightarrow CH_3COOH$	60	0.019	Davidovits et al. (1995)
20[b]	$CH_3COOH \rightarrow CH_3COOH(g)$	5.50×10^3	−5894	Khan and Brimblecombe (1992)
21[a]	$NO_3(g) \rightarrow NO_3$	62	4×10^{-3}	Kirchner et al. (1990); Rudich et al. (1996)
22[b]	$NO_3 \rightarrow NO_3(g)$	0.6	0	Rudich et al. (1996)
23[a]	$N_2O_5(g) \rightarrow N_2O_5$	108	3.7×10^{-3}	George et al. (1994)
24[b]	$N_2O_5 \rightarrow N_2O_5(g)$	1.4	0	Herrmann et al. (2000)
25[a]	$NO_2(g) \rightarrow NO_2$	46	2×10^{-4}	Shao et al. (2019)
26[b]	$NO_2 \rightarrow NO_2(g)$	1.0×10^{-2}	−2518	Sander (1999); Pandis and Seinfeld (1989)
27[a]	$HO_2NO_2(g) \rightarrow HO_2NO_2$	79	0.1	Jacob (1986)
28[b]	$HO_2NO_2 \rightarrow HO_2NO_2(g)$	1×10^5	0	Herrmann et al. (2000)
29[a]	$NO(g) \rightarrow NO$	30	0.1	Estimated
30[b]	$NO \rightarrow NO(g)$	1.9×10^{-3}	−1460	Sander (1999); Pandis and Seinfeld (1989)
31[a]	$O_2(g) \rightarrow O_2$	32	0.1	Estimated
32[b]	$O_2 \rightarrow O_2(g)$	1.3×10^{-3}	0	Sander (1999)

[a] Reaction rate constant is $k = \frac{3D_g \mathrm{LWC}}{\Lambda r^2}$. The unit is per second (hereafter s^{-1}). Gas-phase diffusion coefficient is $D_g = \frac{9.45\times10^{17}}{[M]}\sqrt{T(0.03472+\frac{1}{k_1})}$. LWC is the volume mixing ratio of cloud liquid water. $\Lambda = 1+(\lambda+1.3(\frac{1}{k_2}-1))$, $\lambda = \frac{0.71+1.3\beta}{1+\beta}$, $\beta = 4.54\times10^{-15}\sqrt{V_g^2+V_{air}^2}$, $V_g = \sqrt{\frac{8RT}{\pi k_1}}$, $V_{air} = \sqrt{\frac{8RT}{28.8\pi}}$, $R = 8.31\times10^7$ is the ideal gas constant (multiplied by a factor to keep V_g and V_{air} in the unit of centimeters per second; hereafter $cm\,s^{-1}$), r is the radius of cloud droplets in centimeters (hereafter cm), and $[M]$ is the number density of air in the unit of molecules per cubic centimeter (hereafter $molec.\,cm^{-3}$). T is atmospheric temperature in Kelvin (K). k_1 is the molar mass (grams per mole; hereafter $g\,mol^{-1}$). k_2 is the mass accommodation coefficients. All the formulas above refer to Shao et al. (2019) and Liang and Jacobson (1999).
[b] Reaction rate constant is $k = \frac{k_{n-1}}{0.0827T\,\mathrm{LWC}\,C}$. The unit is s^{-1}. $C = k_1\exp(-500k_2(\frac{1}{T}-\frac{1}{298}))$, and k_{n-1} is the rate constant of its reverse reaction with [a]. LWC is as in [a]. k_1 is Henry's law constants (moles per liter per atmosphere; hereafter $M\,atm^{-1}$) are at 298 K. k_2 is ΔH (joules per mole; hereafter $J\,mol^{-1}$)/R (joules per mole per Kelvin; hereafter $J\,mol^{-1}\,K^{-1}$). ΔH is the enthalpy of dissolution. All the formulas above refer to Liang and Jacobson (1999).
[c] All species are liquid species by default, and gas species are marked with (g). The same below.

Table 2. Aqueous-phase chemistry.

No.	Reactions	k_{298}, $M^{-n}s^{-1}$ [a]	E_a/R, K	Reference
	Aqueous ionization equilibria			
33	$H_2O_2 \rightarrow H^+ + HO_2^-$	1.26×10^{-2}		De Laat and Le (2005)
34	$H^+ + HO_2^- \rightarrow H_2O_2$	10^{10}		De Laat and Le (2005)
35	$HO_2 \rightarrow H^+ + O_2^-$	1.14×10^6		Miller et al. (2013)
36	$H^+ + O_2^- \rightarrow HO_2$	7.2×10^{10}		Miller et al. (2013)
37	$CO_2 + H_2O \rightarrow H^+ + HCO_3^-$	3.84×10^4	9250	Welch et al. (1969); Graedel and Weschler (1981)
38	$H^+ + HCO_3^- \rightarrow CO_2 + H_2O$	5×10^{10}		Graedel and Weschler (1981)
39	$HCO_3^- \rightarrow H^+ + CO_3^{2-}$	2.35	1820	Harned and Owen (1958)
40	$H^+ + CO_3^{2-} \rightarrow HCO_3^-$	5×10^{10}		Graedel and Weschler (1981)
41	$NH_3 + H_2O \rightarrow NH_4^+ + OH^-$	6.02×10^5	560	Harned and Owen (1958)
42	$NH_4^+ + OH^- \rightarrow NH_3 + H_2O$	3.4×10^{10}		Graedel and Weschler (1981)
43	$HNO_3 \rightarrow H^+ + NO_3^-$	1.1×10^{12}	−1800	Redlich (1946)
44	$H^+ + NO_3^- \rightarrow HNO_3$	5×10^{10}		Graedel and Weschler (1981)
45	$HNO_2 \rightarrow H^+ + NO_2^-$	2.65×10^7	1760	Park and Lee (1988)
46	$H^+ + NO_2^- \rightarrow HNO_2$	5×10^{10}		Graedel and Weschler (1981)
47	$HO_2NO_2 \rightarrow H^+ + O_2NO_2^-$	5×10^5		Lammel et al. (1990)
48	$H^+ + O_2NO_2^- \rightarrow HO_2NO_2$	5×10^{10}		Herrmann et al. (2000)
49	$SO_2 + H_2O \rightarrow H^+ + HSO_3^-$	6.27×10^4	−1940	Beilke and Gravenhorst (1978); Harned and Owen (1958)
50	$H^+ + HSO_3^- \rightarrow SO_2 + H_2O$	2.0×10^8		Graedel and Weschler (1981)
51	$HSO_3^- \rightarrow H^+ + SO_3^{2-}$	3110	−1960	Beilke and Gravenhorst (1978)
52	$H^+ + SO_3^{2-} \rightarrow HSO_3^-$	5×10^{10}		Graedel and Weschler (1981)
53	$HSO_4^- \rightarrow H^+ + SO_4^{2-}$	1.02×10^9	−2700	Redlich (1946)
54	$H^+ + SO_4^{2-} \rightarrow HSO_4^-$	1×10^{11}		Graedel and Weschler (1981)
55	$HCOOH \rightarrow H^+ + HCOO^-$	8.85×10^6	−12	Harned and Owen (1958)
56	$H^+ + HCOO^- \rightarrow HCOOH$	5×10^{10}		Graedel and Weschler (1981)
57	$CH_3COOH \rightarrow H^+ + CH_3COO^-$	8.75×10^5	−46	Harned and Owen (1958)
58	$H^+ + CH_3COO^- \rightarrow CH_3COOH$	5×10^{10}		Graedel and Weschler (1981)
	HO_x chemistry			
59	$H_2O_2 \xrightarrow{h\nu} 2\,OH$	See ref.		Zellner et al. (1990)
60	$O_3 \xrightarrow{H_2O,h\nu} H_2O_2 + O_2$	See ref.		Graedel and Weschler (1981)
61	$OH + HO_2 \rightarrow H_2O + O_2$	6.6×10^9	1500	Sehested et al. (1968); Thomas (1963)
62	$HO_2 + HO_2 \rightarrow H_2O_2 + O_2$	8.3×10^5	2700	Bielski et al. (1985)
63	$OH + H_2O_2 \rightarrow HO_2 + H_2O$	2.7×10^7	1700	Christensen et al. (1982); Buxton et al. (1988b)
64	$O_2^- + O_3 \xrightarrow{H_2O} OH + OH^- + 2\,O_2$	1.5×10^9	1500	Sehested et al. (1983); Bielski et al. (1985)
65	$OH + HSO_3^- \xrightarrow{O_2} SO_5^- + H_2O$	4.5×10^9	1500	Huie and Neta (1987)
66	$OH + SO_3^{2-} \xrightarrow{O_2} SO_5^- + OH^-$	5.5×10^9	1500	Huie and Neta (1987); Adams and Boag (1964); Buxton et al. (1988b)
67	$HCOO^- + OH \xrightarrow{O_2} CO_2 + HO_2 + OH^-$	3.2×10^9	1250	Chin and Wine (1994)
68	$SO_3^{2-} + SO_4^- \xrightarrow{O_2} SO_4^{2-} + SO_5^-$	7.5×10^8	1500	Wine et al. (1989)
69	$HSO_3^- + SO_4^- \xrightarrow{O_2} SO_4^{2-} + SO_5^- + H^+$	7.5×10^8	1500	Wine et al. (1989)
70	$HSO_3^- + O_3 \rightarrow SO_4^{2-} + H^+ + O_2$	3.7×10^5	5530	Hoffmann (1986); Wine et al. (1989)
71	$SO_3^{2-} + O_3 \rightarrow SO_4^{2-} + O_2$	1.5×10^9	5280	Hoffmann (1986); Wine et al. (1989)
72	$SO_4^- + OH^- \rightarrow SO_4^{2-} + OH$	8.0×10^7	1500	Maruthamuthu and Neta (1978)
73	$SO_4^- + H_2O_2 \rightarrow H^+ + SO_4^{2-} + HO_2$	1.2×10^7	2000	Wine et al. (1989)
74	$SO_4^- (+ H_2O) \rightarrow SO_4^{2-} + H^+ + OH$	440	1850	Bao and Barker (1996)
75	$SO_4^- + HCOO^- \xrightarrow{O_2} SO_4^{2-} + CO_2 + HO_2$	1.1×10^8	1500	Reese et al. (1997); Wine et al. (1989)
76	$HCOOH + OH \xrightarrow{O_2} H_2O + CO_2 + HO_2$	1.1×10^8	1000	Chin and Wine (1994)
77	$O_3 + H_2O_2 + OH^- \rightarrow OH + O_2^- + O_2 + H_2O$	4.4×10^8	−4000	Staehelin and Hoigne (1982)

Table 2. Continued.

No.	Reactions	k_{298}, $M^{-n}\,s^{-1}$ [a]	E_a/R, K	Reference
78	$SO_4^- + HO_2 \rightarrow SO_4^{2-} + H^+ + O_2$	5.0×10^9	1500	Jacob (1986)
79	$SO_4^- + O_2^- \rightarrow SO_4^{2-} + O_2$	5.0×10^9	1500	Jacob (1986)
80	$HCOO^- + O_3 \rightarrow CO_2 + OH + O_2^-$	1.0×10^2	5500	Hoigne and Bader (1983b)
81	$SO_5^- + HCOO^- \xrightarrow{O_2} HSO_5^- + CO_2 + O_2^-$	1.4×10^4	4000	Jacob (1986)
82	$SO_5^- + HSO_3^- \xrightarrow{O_2} HSO_5^- + SO_5^-$	2.5×10^4	3850	Huie and Neta (1987)
83	$HSO_5^- + OH \rightarrow SO_5^- + H_2O$	1.7×10^7	1900	Maruthamuthu and Neta (1977)
84	$HSO_5^- + HSO_3^- + H^+ \rightarrow 2\,SO_4^{2-} + 3\,H^+$	1.7×10^7	2000	Mcelroy (1987); Betterton and Hoffmann (1988)
85	$SO_5^- + HSO_3^- \rightarrow SO_4^- + SO_4^{2-} + H^+$	7.5×10^4	3500	Huie and Neta (1987)
86	$O_2^- + SO_5^- \xrightarrow{H_2O} O_2 + HSO_5^- + OH^-$	1.0×10^8	1050	Jacob (1986)
87	$OH + HSO_3^- \xrightarrow{O_2} SO_4^{2-} + H^+ + HO_2$	4.5×10^9		Huie and Neta (1987)
88	$OH + O_3 \rightarrow HO_2 + O_2$	2.0×10^9		Buhler et al. (1984)
89	$HO_2 + O_2^- \xrightarrow{H^+} H_2O_2 + O_2$	9.7×10^7	1060	Bielski et al. (1985)
90	$O_2^- + OH \rightarrow OH^- + O_2$	1.1×10^{10}	2120	Christensen et al. (1989)
91	$HSO_3^- + OH \rightarrow H_2O + SO_3^-$	2.7×10^9		Buxton et al. (1996b)
92	$SO_3^{2-} + OH \rightarrow OH^- + SO_3^-$	4.6×10^9		Buxton et al. (1996b)
93	$HSO_3^- + H_2O_2 + H^+ \rightarrow SO_4^{2-} + H_2O + 2\,H^+$	6.9×10^7	4000	Lind et al. (1987)
94	$SO_2 + O_3 \xrightarrow{H_2O} HSO_4^- + O_2 + H^+$	2.4×10^4		Hoffmann (1986)
95	$SO_5^- + SO_5^- \rightarrow S_2O_8^{2-} + O_2$	1.8×10^8	2600	Herrmann et al. (1995)
96	$SO_5^- + SO_5^- \rightarrow 2\,SO_4^- + O_2$	7.2×10^6	2600	Herrmann et al. (1995)
97	$SO_5^- + HO_2 \rightarrow HSO_5^- + O_2$	1.7×10^9		Buxton et al. (1996a)
98	$SO_3^- + O_2 \rightarrow SO_5^-$	2.5×10^9		Buxton et al. (1996b)
99	$SO_5^- + HSO_3^- \rightarrow HSO_5^- + SO_3^-$	8.6×10^3		Buxton et al. (1996b)
100	$SO_5^- + SO_3^{2-} \xrightarrow{H^+} HSO_5^- + SO_3^-$	2.13×10^5		Buxton et al. (1996b)
101	$SO_5^- + SO_3^{2-} \rightarrow SO_4^- + SO_4^{2-}$	5.5×10^5		Buxton et al. (1996b)
102	$OH + HSO_4^- \rightarrow H_2O + SO_4^-$	3.5×10^5		Tang et al. (1988)
103	$SO_4^- + HSO_3^- \rightarrow SO_4^{2-} + SO_3^- + H^+$	3.2×10^8		Reese et al. (1997)
104	$SO_4^- + SO_3^{2-} \rightarrow SO_4^{2-} + SO_3^-$	3.2×10^8	1200	Reese et al. (1997)
105	$HSO_5^- + SO_3^{2-} + H^+ \rightarrow 2\,SO_4^{2-} + 2\,H^+$	7.14×10^6		Betterton and Hoffmann (1988)
106	$HCOOH + SO_4^- \xrightarrow{O_2} SO_4^{2-} + H^+ + HO_2 + CO_2$	2.5×10^6		Reese et al. (1997)
107	$O_2^- + H_2O_2 \rightarrow OH^- + OH + O_2$	0.13		Bielski et al. (1985)
108	$OH + OH \rightarrow H_2O_2$	5.5×10^9		Miller et al. (2013)
109	$H_2O_2 + HO_2 \rightarrow H_2O + O_2 + OH$	3.1		Miller et al. (2013)
110	$HO_2 + O_2^- \rightarrow HO_2^- + O_2$	9.7×10^7		De Laat and Le (2005)
111	$O_2^{2-} + H^+ \rightarrow HO_2^-$	10^{10}		De Laat and Le (2005)
112	$SO_4^- + SO_4^- \rightarrow S_2O_8^{2-}$	4.5×10^8		Buxton et al. (1996b)
113	$OH^- + O_3 \xrightarrow{H_2O} H_2O_2 + O_2 + OH^-$	70		Staehelin and Hoigne (1982)
114	$HO_2^- + O_3 \rightarrow OH + O_2^- + O_2$	2.8×10^6	2500	Staehelin and Hoigne (1982)
115	$H_2O_2 + O_3 \rightarrow H_2O + 2\,O_2$	$7.8 \times 10^{-3}[O_3]^{-0.5}$		Martin et al. (1981)
116	$HCOOH + O_3 \rightarrow CO_2 + HO_2 + OH$	5.0	0	Hoigne and Bader (1983a)
117	$SO_2 + H_2O_2 \xrightarrow{H_2O} SO_4^{2-} + 2\,H^+ + H_2O$	7.5×10^7	4430	Mcardle and Hoffmann (1983)
118	$SO_3^{2-} + H_2O_2 \rightarrow SO_4^{2-} + H_2O$	7.5×10^7	4430	Mcardle and Hoffmann (1983)
119	$SO_5^- + SO_3^{2-} \xrightarrow{O_2,H_2O} HSO_5^- + SO_5^- + OH^-$	2.5×10^4	2000	Huie and Neta (1987)
120	$SO_5^- + HCOOH \xrightarrow{O_2} HSO_5^- + CO_2 + HO_2$	200	5300	Jacob (1986)
121	$SO_2 + HO_2 \xrightarrow{H_2O} SO_4^{2-} + OH + 2\,H^+$	1.0×10^6	0	Hoffman and Calvert (1985)
122	$HSO_3^- + HO_2 \rightarrow SO_4^{2-} + OH + H^+$	1.0×10^6	0	Hoffman and Calvert (1985)
123	$SO_3^{2-} + HO_2 \rightarrow SO_4^{2-} + OH$	1.0×10^6	0	Hoffman and Calvert (1985)
124	$SO_2 + O_2^- \xrightarrow{H_2O} SO_4^{2-} + OH + H^+$	1.0×10^5	0	Hoffman and Calvert (1985)
125	$HSO_3^- + O_2^- \rightarrow SO_4^{2-} + OH$	1.0×10^5	0	Hoffman and Calvert (1985)
126	$SO_3^{2-} + O_2^- \xrightarrow{H_2O} SO_4^{2-} + OH + OH^-$	1.0×10^5	0	Hoffman and Calvert (1985)
127	$SO_3^- + SO_3^- \xrightarrow{H_2O} SO_3^{2-} + H^+ + HSO_4^-$	0.37		Fischer and Warneck (1996)

Table 2. Continued.

No.	Reactions		k_{298}, $M^{-n}\,s^{-1}$ [a]	E_a/R, K	Reference
	Fe chemistry				
128	$FeOH^{2+} \xrightarrow{h\nu} Fe^{2+} + OH$		See ref.		Benkelberg and Warneck (1995)
129	$FeSO_4^+ \xrightarrow{h\nu} Fe^{2+} + SO_4^-$		See ref.		Benkelberg and Warneck (1995)
130	$H_2O_2 + Fe^{2+} \rightarrow FeOH^{2+} + OH$	$63 + (3 \times 10^{-10}$	$[H^+]^{-1}\ 5.9 \times 10^6)$		Millero and Sotolongo (1989)
131	$Fe^{2+} + O_3 \xrightarrow{H_2O} FeOH^{2+} + OH + O_2$		8.2×10^5		Logager et al. (1992)
132	$FeOH^{2+} + HSO_3^- \xrightarrow{O_2} Fe^{2+} + SO_4^{2-} + H_2O$	$[FeOH^{2+}]$	$\times 1 \times 10^9$		Martin et al. (1991)
133	$O_3 + Fe^{2+} \rightarrow FeO^{2+} + O_2$		8.2×10^5		Logager et al. (1992)
134	$H_2O_2 + FeO^{2+} \rightarrow FeOH^{2+} + HO_2$		9.5×10^3	2800	Jacobsen et al. (1997)
135	$HO_2 + FeO^{2+} \rightarrow FeOH^{2+} + O_2$		2.0×10^6		Jacobsen et al. (1997)
136	$OH + FeO^{2+} \xrightarrow{H_2O} FeOH^{2+} + H_2O_2$		1.0×10^7		Logager et al. (1992); Jacobsen et al. (1997)
137	$FeO^{2+} + H_2O \rightarrow FeOH^{2+} + OH$		1.3×10^{-2}	4100	Jacobsen et al. (1997)
138	$FeO^{2+} + Fe^{2+} \xrightarrow{H_2O} 2\ FeOH^{2+}$		7.2×10^4	840	Jacobsen et al. (1997)
139	$FeO^{2+} + Fe^{2+} \xrightarrow{H_2O} Fe(OH)_2Fe^{4+}$		1.8×10^4	5050	Jacobsen et al. (1997)
140	$Fe(OH)_2Fe^{4+} \rightarrow 2\ FeOH^{2+}$		0.49	8800	Jacobsen et al. (1997)
141	$HNO_2 + FeO^{2+} \rightarrow FeOH^{2+} + NO_2$		1.1×10^4	4150	Jacobsen et al. (1998)
142	$NO_2^- + FeO^{2+} \xrightarrow{H^+} FeOH^{2+} + NO_2$		1.0×10^5		Jacobsen et al. (1998)
143	$HSO_3^- + FeO^{2+} \rightarrow FeOH^{2+} + SO_3^-$		2.5×10^5		Jacobsen et al. (1998)
144	$HCOOH + FeO^{2+} \xrightarrow{O_2} FeOH^{2+} + CO_2 + HO_2$		160	2680	Jacobsen et al. (1998)
145	$HCOO^- + FeO^{2+} \xrightarrow{H^+, O_2} FeOH^{2+} + CO_2 + HO_2$		3.0×10^5		Jacobsen et al. (1998)
146	$FeOH^{2+} + HSO_3^- \rightarrow FeSO_3^+ + H_2O$		4.0×10^6		Lente and Fabian (2002)
147	$FeSO_3^+ + H^+ \xrightarrow{OH^-} FeOH^{2+} + HSO_3^-$		2.08×10^3		Lente and Fabian (2002)
148	$FeSO_3^+ \rightarrow Fe^{2+} + SO_3^-$		0.19		Lente and Fabian (2002)
149	$Fe^{2+} + SO_3^- \rightarrow FeSO_3^+$		3.0×10^6	5605	Buxton et al. (1999)
150	$FeOH^{2+} + SO_3^- \rightarrow Fe^{2+} + HSO_4^-$	$3.0 \times 10^5 + 7.6 \times 10^6 \times 1.64 \times 10^{-3}$	$[H^+]^{-1}$		Warneck (2018)
151	$OH + Fe^{2+} \rightarrow FeOH^{2+}$		4.3×10^8	1100	Christensen and Sehested (1981)
152	$H_2O_2 + FeOH^{2+} \rightarrow HO_2 + H_2O + Fe^{2+}$		2×10^{-3}		Walling and Goosen (1973)
153	$O_2^- + FeOH^{2+} \rightarrow O_2 + Fe^{2+} + OH^-$		1.5×10^8		Rush and Bielski (1985)
154	$HO_2 + FeOH^{2+} \rightarrow Fe^{2+} + O_2 + H_2O$		1.3×10^5		Ziajka et al. (1994)
155	$O_2^- + Fe^{2+} \xrightarrow{H^+, H_2O} H_2O_2 + FeOH^{2+}$		1.0×10^7		Rush and Bielski (1985)
156	$HO_2 + Fe^{2+} \xrightarrow{H_2O} H_2O_2 + FeOH^{2+}$		1.2×10^6	5050	Jayson et al. (1973)
157	$NO_3 + Fe^{2+} \xrightarrow{OH^-} NO_3^- + FeOH^{2+}$		8×10^6		Pikaev et al. (1974)
158	$FeOH^{2+} + HSO_3^- \rightarrow Fe^{2+} + SO_3^- + H_2O$		39		Ziajka et al. (1994)
159	$Fe^{2+} + SO_5^- \xrightarrow{H_2O} FeOH^{2+} + HSO_5^-$		4.3×10^7		Herrmann et al. (1996)
160	$Fe^{2+} + HSO_5^- \rightarrow FeOH^{2+} + SO_4^-$		3×10^4		Ziajka et al. (1994)
161	$Fe^{2+} + SO_4^- \xrightarrow{H_2O} FeOH^{2+} + SO_4^{2-} + H^+$		3.5×10^7		Ziajka et al. (1994)
162	$Fe^{2+} + S_2O_8^{2-} \xrightarrow{H_2O} FeOH^{2+} + SO_4^{2-} + SO_4^- + H^+$		17		Buxton et al. (1997)
163	$SO_4^- + Fe^{2+} \rightarrow FeSO_4^+$		3×10^8		Mcelroy and Waygood (1990)
164	$FeOH^{2+} + SO_4^{2-} \rightarrow FeSO_4^+ + OH^-$		3.2×10^3		Brandt and Vaneldik (1995)
165	$FeSO_4^+ \xrightarrow{OH^-} FeOH^{2+} + SO_4^{2-}$		1.8×10^5		Brandt and Vaneldik (1995)
166	$Fe^{2+} + O_2 \xrightarrow{OH^-} FeOH^{2+} + O_2^-$		8.8×10^{-2}		Santana-Casiano et al. (2005)
167	$Fe^{2+} + O_2^- \xrightarrow{OH^-} FeOH^{2+} + O_2^{2-}$		10^7		De Laat and Le (2005)
168	$O_2^- + FeSO_4^+ \rightarrow Fe^{2+} + SO_4^{2-} + O_2$		1.5×10^8		Rush and Bielski (1985)
169	$HO_2 + FeSO_4^+ \rightarrow Fe^{2+} + SO_4^{2-} + O_2 + H^+$		1.0×10^3		Rush and Bielski (1985)
170	$Fe^{2+} + H_2O_2 \rightarrow FeO^{2+} + H_2O$		See ref.		Tong et al. (2017)
	N chemistry				
171	$NO_2^- \xrightarrow{H^+, h\nu} NO + OH$		See ref.		Zellner et al. (1990)
172	$NO_3 \xrightarrow{H^+, h\nu} NO_2 + OH$		See ref.		Zellner et al. (1990)
173	$N_2O_5 + H_2O \rightarrow 2\ H^+ + 2\ NO_3^-$		5×10^9		Herrmann et al. (2000)
174	$NO_3 + OH^- \rightarrow NO_3^- + OH$		9.4×10^7	2700	Exner et al. (1992)
175	$NO_3 + H_2O_2 \rightarrow NO_3^- + H^+ + HO_2$		4.9×10^6	2000	Herrmann et al. (1994)

Table 2. Continued.

No.	Reactions	k_{298}, $M^{-n}\,s^{-1}$ [a]	E_a/R, K	Reference
176	$NO_3 + HSO_3^- \rightarrow NO_3^- + H^+ + SO_3^-$	1.3×10^9	2000	Exner et al. (1992)
177	$NO_3 + SO_3^{2-} \rightarrow NO_3^- + SO_3^-$	3.0×10^8		Exner et al. (1992)
178	$NO_3 + HSO_4^- \rightarrow NO_3^- + H^+ + SO_4^-$	2.6×10^5		Raabe (1996)
179	$NO_3 + SO_4^{2-} \rightarrow NO_3^- + SO_4^-$	5.6×10^3		Logager et al. (1993)
180	$NO_2 + OH \rightarrow NO_3^- + H^+$	1.2×10^{10}		Wagner et al. (1980)
181	$NO_2 + O_2^- \rightarrow NO_2^- + O_2$	1×10^8		Warneck and Wurzinger (1988)
182	$NO_2 + NO_2 \xrightarrow{H_2O} HNO_2 + NO_3^- + H^+$	8.4×10^7	−2900	Park and Lee (1988)
183	$O_2NO_2^- \rightarrow NO_2^- + O_2$	4.5×10^{-2}		Lammel et al. (1990)
184	$NO_2^- + NO_3 \rightarrow NO_3^- + NO_2$	1.4×10^9	0	Herrmann and Zellner (1998)
185	$SO_4^- + NO_3^- \rightarrow SO_4^{2-} + NO_3$	5.0×10^4		Exner et al. (1992)
186	$HCOOH + NO_3 \xrightarrow{O_2} NO_3^- + H^+ + HO_2 + CO_2$	3.8×10^5	3400	Exner et al. (1994)
187	$HCOO^- + NO_3 \xrightarrow{O_2} NO_3^- + HO_2 + CO_2$	5.1×10^7	2200	Exner et al. (1994)
188	$NO_2 + HO_2 \rightarrow HO_2NO_2$	1.0×10^7		Warneck and Wurzinger (1988)
189	$HO_2NO_2 \rightarrow NO_2 + HO_2$	4.6×10^{-3}		Warneck and Wurzinger (1988)
190	$SO_4^- + NO_2^- \rightarrow SO_4^{2-} + NO_2$	9.8×10^8	1500	Wine et al. (1989)
191	$NO + NO_2 \xrightarrow{H_2O} 2\,NO_2^- + 2\,H^+$	2.0×10^8	1500	Lee (1984)
192	$NO + OH \rightarrow NO_2^- + H^+$	2.0×10^{10}	1500	Strehlow and Wagner (1982)
193	$HNO_2 + OH \rightarrow NO_2 + H_2O$	1.0×10^9	1500	Rettich (1978)
194	$NO_2^- + OH \rightarrow NO_2 + OH^-$	1.0×10^{10}	1500	Treinin and Hayon (1970)
195	$HNO_2 + H_2O_2 \xrightarrow{H^+} NO_3^- + 2\,H^+ + H_2O$	$6.3 \times 10^3\ [H^+]$	6693	Lee and Lind (1986)
196	$NO_2^- + O_3 \rightarrow NO_3^- + O_2$	5.0×10^5	6950	Damschen and Martin (1983)
197	$NO_3 + HO_2 \rightarrow NO_3^- + H^+ + O_2$	4.5×10^9	1500	Jacob (1986)
198	$NO_3 + O_2^- \rightarrow NO_3^- + O_2$	1.0×10^9	1500	Jacob (1986)
199	$2\,NO_2 + HSO_3^- \xrightarrow{H_2O} SO_4^{2-} + 3\,H^+ + 2\,NO_2^-$	2.0×10^6	0	Lee and Schwartz (1983)[c]
200	$NO_2 + NO_2 \rightarrow N_2O_4$	4.5×10^8 [b]		Graedel and Weschler (1981)
201	$N_2O_4 \xrightarrow{H_2O} 2\,H^+ + NO_2^- + NO_3^-$	1.0×10^3 [b]		Graedel and Weschler (1981)
202	$NO_3 + H_2O \rightarrow NO_3^- + OH + H^+$	6.0	4500	Rudich et al. (1996)
203	$NO_3^- + OH + H^+ \rightarrow NO_3 + H_2O$	1.4×10^8		Rudich et al. (1996)
204	$HSO_5^- + NO_2^- \rightarrow HSO_4^- + NO_3^-$	0.31	6646	Edwards and Mueller. (1962)
205	$HO_2NO_2 + HSO_3^- \rightarrow HSO_4^- + NO_3$	3.5×10^5		Amels et al. (1996)
	Carbonate chemistry			
206	$HCO_3^- + O_2^- \rightarrow HO_2^- + CO_3^-$	1.5×10^6	0	Schmidt (1972)
207	$CO_3^- + H_2O_2 \rightarrow HO_2 + HCO_3^-$	8.0×10^5	2820	Behar et al. (1970)
208	$CO_2^- + O_2 \rightarrow O_2^- + CO_2$	2.4×10^9		Tan et al. (2009)
209	$CO_3^- + O_2^- \rightarrow CO_3^{2-} + O_2$	6.8×10^8		Tan et al. (2009)
210	$CO_3^- + HCOO^- \rightarrow HCO_3^- + CO_2^-$	1.5×10^5		Tan et al. (2009)
211	$NO_2^- + CO_3^- \rightarrow CO_3^{2-} + NO_2$	6.6×10^5	850	Huie et al. (1991)
212	$HCOO^- + CO_3^- \xrightarrow{O_2} CO_3^{2-} + HO_2 + CO_2$	1.4×10^5	3300	Zellner et al. (1996)
213	$HCO_3^- + OH \rightarrow H_2O + CO_3^-$	1.7×10^7	1900	Exner (1990)
214	$CO_3^{2-} + OH \rightarrow OH^- + CO_3^-$	3.9×10^8	2840	Buxton et al. (1988b, a)
215	$CO_3^{2-} + SO_4^- \rightarrow SO_4^{2-} + CO_3^-$	4.1×10^7		Herrmann et al. (2000)
216	$HCO_3^- + SO_4^- \rightarrow SO_4^{2-} + CO_3^- + H^+$	2.8×10^6	2090	Huie and Clifton (1990)
217	$CO_3^{2-} + NO_3 \rightarrow NO_3^- + CO_3^-$	4.1×10^7		Herrmann et al. (2000)
218	$CO_3^- + CO_3^- \xrightarrow{O_2} 2\,O_2^- + 2\,CO_2$	2.2×10^6		Huie and Clifton (1990)
219	$CO_3^- + Fe^{2+} \xrightarrow{OH^-} CO_3^{2-} + FeOH^{2+}$	2×10^7		Herrmann et al. (2000)
220	$CO_3^- + HO_2 \rightarrow HCO_3^- + O_2$	6.5×10^8		Herrmann et al. (2000)
221	$CO_3^- + HSO_3^- \rightarrow HCO_3^- + SO_3^-$	1×10^7		Herrmann et al. (2000)
222	$CO_3^- + SO_3^{2-} \rightarrow CO_3^{2-} + SO_3^-$	5.0×10^6	470	Huie et al. (1991)

[a] n is the reaction order −1. The units are s^{-1} for first-order reactions and moles per liter per second (hereafter $M^{-1}\,s^{-1}$) for second-order reactions. Reaction rate constant is $k = k_{298}\exp(-\frac{E_a}{R}(\frac{1}{T} - \frac{1}{298}))$. [b] The temperature for k is 293 K. [c] Referenced from https://www.osti.gov/biblio/6567096 (last access: 27 August 2021).

in Tables 1 and 2, coupled with default gas chemistry. In the non-cloudy part, the calculation is similar to the original case but still without parameterized aqueous-phase reactions. Finally, the concentration in each grid is the average of the cloudy and non-cloudy results weighted by F_{cld}.

The time step used in this study is the default 30 min in CESM2. In the improved case, the lifetime of clouds (i.e., the time between the formation and evaporation of clouds) is set equal to the time step. At $t = 0$ of each time step, all the cloud droplets are assumed to be instantaneously and simultaneously formed according to the cloud-related variables, such as LWC, F_{cld}, and r, and all the water-soluble species (listed in Table 1) are dissolved into the cloud droplets according to the effective Henry's law constants. The pH value of each grid cell is calculated by the ionization equilibria of ionizable species (listed in Table 2) and the dissociation of CCN (including sulfate, nitrate, and ammonium), assuming that equilibrium and electroneutrality are continuously maintained. Such pH values can directly influence the formation of aqueous-phase sulfate and nitrate of this time step. At the same time, a given initial concentration of soluble Fe^{3+} (5 µM) is allocated into each cloud droplet. When $t = 30$ min, all the cloud droplets are assumed to instantaneously evaporate. All the species remaining in the aqueous phase are transferred directly back to the gas phase. Low-volatility species such as ammonium, sulfate, and nitrate are released directly back to the atmosphere as inorganic aerosols. Meanwhile, the newly formed sulfate and nitrate will further influence the ionization equilibria and the calculation of pH values in the next step, thus forming a fully coupled feedback system between pH values and concentrations of sulfate and nitrate.

On the basis of the improved case, more sensitivity cases are simulated to explore the influences of different factors (e.g., the concentration of soluble Fe and the pH value) on the capacity for SO_2 oxidation. The process of all these simulations is the same as that of the improved case. The detailed description of all the model simulations used in this study is summarized in Table S1 in the Supplement.

Finally, all the simulations are running for a 2 year period, from 1 January 2014 to 31 December 2015. The first year is used for model spin-up. In this study, we used the information at https://svn-ccsm-inputdata.cgd.ucar.edu/trunk/inputdata/input/atm/cam/inic/fv/ (cami-chem_1990-01-01_0.9x1.25_L30_c080724.nc, last access: 31 December 2021) as the initial data and boundary conditions to provide the initial values of all the physical variables and concentrations of all the chemical species. The output of the simulation is in the form of a daily mean and is then converted to a monthly or seasonal mean for research needs.

2.4 Observations for evaluation of global simulation

For the model evaluation, the observational data used in this study are collected from four monitoring networks. The observations in Europe (EU) are obtained from the European Monitoring and Evaluation Programme (EMEP, 2020; https://www.emep.int/, last access: 8 August 2020). The observations in the United States of America (USA) are obtained from the U.S. Environmental Protection Agency Air Quality System (United States Environmental Protection Agency, 2020; https://aqs.epa.gov/aqsweb/airdata/download_files.html#Raw, last access: 19 July 2020). The observations in China (CN) are obtained from the China National Environmental Monitoring Center (CNEMC; https://quotsoft.net/air/, last access: 22 December 2020). The observations in Japan and South Korea (JK) are obtained from the Acid Deposition Monitoring Network in East Asia (EANET; https://monitoring.eanet.asia/document/public/index, last access: 2 November 2020). The locations of monitoring stations are shown in Fig. 1. All observational data were collected from 1 January 2015 to 31 December 2015. The monthly averages used for analysis of the results are calculated from raw daily averages or even hourly averages collected from the measurement networks above. For convenience of comparison, the units of simulated concentration of SO_2 are all converted to the forms in corresponding observational data.

3 Effects of in-cloud aqueous-phase chemical mechanisms on the simulation of SO_2

3.1 Simulation of SO_2 in the original case

Figure 2 shows the seasonally averaged surface mixing ratios of SO_2 in the original simulation. There are huge spatial and temporal differences in the global distribution of SO_2. On the one hand, the mixing ratios of SO_2 are no more than 0.1 ppbv in most parts of the world and are basically concentrated in Asia, EU, North America (NA), and southern Africa (SA) and especially in central and eastern CN. The mixing ratios in NA and EU are mainly in the ranges of 0.1–5 and 1–10 ppbv, respectively. The mixing ratios in EU are slightly higher than those in NA. Meanwhile, the mixing ratios in the eastern USA are evidently higher than those in the western USA. In EA, the mixing ratios in JK range from 0.1 to 5 ppbv throughout the year. The mixing ratios in most of central and eastern CN are in the range of 10–50 ppbv and are even higher than 50 ppbv in some regions, which are much higher than those in other regions. In addition, similar to the USA, the mixing ratios in central and eastern CN are much higher than those in western CN. Such distributions are directly related to the high emissions of SO_2 in these regions of CN (Jo et al., 2020; Xie et al., 2016; Geng et al., 2019).

On the other hand, the mixing ratios of SO_2 are remarkably different in the four seasons. They are highest in winter, followed by spring and autumn, and lowest in summer, especially in Asia and NA. Such seasonal differences are related to both emissions and the capacity for SO_2 oxidation in the

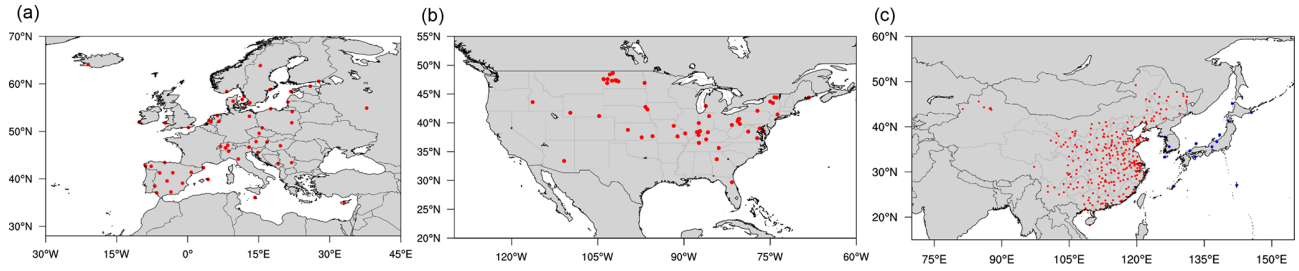

Figure 1. Locations of monitoring sites from various measurement networks in **(a)** Europe (EU; EMEP), **(b)** USA (EPA), and **(c)** East Asia (EA; red points for CNEMC and blue points for EANET).

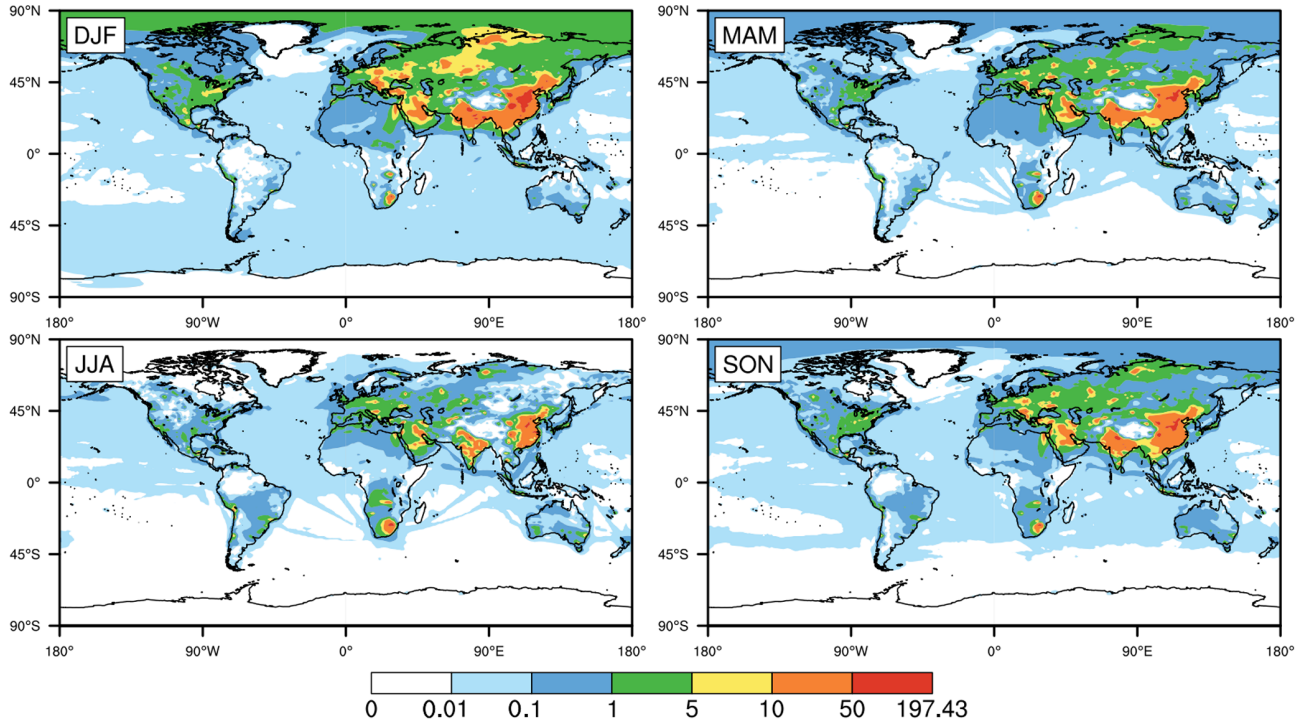

Figure 2. Global distribution of seasonally averaged surface mixing ratios of SO_2 (in parts per billion by volume; hereafter ppbv) in 2015, simulated by CESM2 with standard configuration (i.e., the original case). DJF, MAM, JJA, and SON represent December–January–February, March–April–May, June–July–August and September–October–November, respectively, with the same below.

gas phase. In winter, due to the increase in heating demand, the combustion of fossil fuels such as coal could significantly increase the emissions of SO_2 (Jo et al., 2020; Xie et al., 2016; Geng et al., 2019; Feng et al., 2020). At the same time, higher temperatures and stronger sunlight could enhance the gas-phase oxidation of SO_2 in summer, which is the opposite in winter. Such phenomena are consistent with multiple studies (Alexander et al., 2009; Huang et al., 2014; Tilgner et al., 2013; Shao et al., 2019).

3.2 Differences between the original and improved simulations

After replacement of default parameterized aqueous-phase reactions with detailed in-cloud aqueous-phase chemistry, the surface mixing ratios of SO_2 generally decrease markedly, as shown in Fig. 3. The extent of the reduction is distinct in different regions and seasons. In general, reductions in SO_2 mainly occur in Asia, EU, NA, and SA. The mixing ratios of SO_2 decrease the most in CN, followed by EU, and the least in NA and JK. These results are partly due to the relatively high background mixing ratios in these regions in the original simulation. Therefore, all the distribution patterns above are also similar to those in the original simulation. The reductions in SO_2 also differ in various seasons. In NA and EU, the mixing ratios of SO_2 in most regions are reduced by 0.1–5 and 1–10 ppbv in winter, respectively. In spring and autumn, the mixing ratios mainly decrease by 0.1–5 ppbv, which is slightly less than that in winter. How-

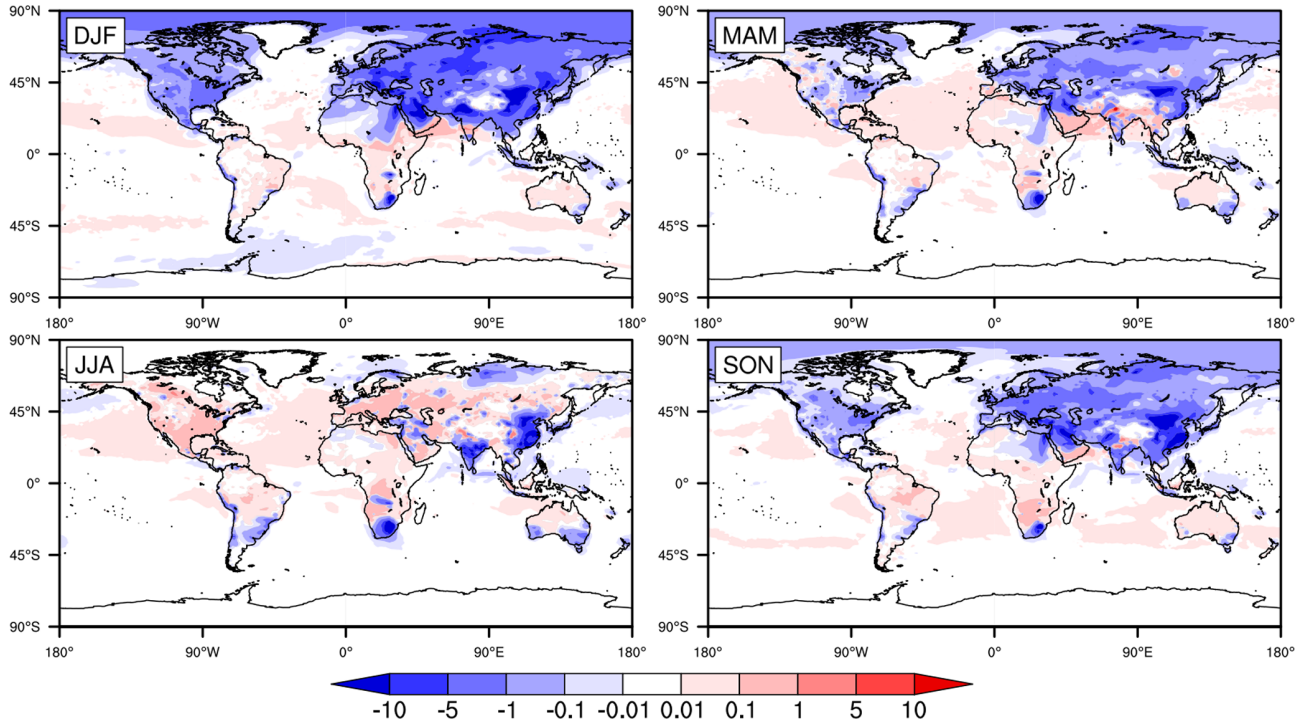

Figure 3. The differences in global seasonally averaged surface SO_2 mixing ratios between the improved case and the original case in 2015, after the incorporation of detailed in-cloud aqueous-phase chemical mechanisms (ppbv).

ever, the reduction in SO_2 in summer is very limited. Notably, the mixing ratios in some areas even increase slightly, which is partly due to the replacement of the default parameterized aqueous-phase reactions. Sometimes these simplified and parameterized reactions are even stronger than detailed radical reactions, especially in summer. Similar to Fig. 2, Fig. 3 shows that the decline in SO_2 mixing ratios in the eastern USA is larger than that in the western USA, which is also related to the background mixing ratios in the original case. However, the situation is different in EA. The mixing ratios decrease significantly in all seasons in central and eastern CN. The reduction is always more than 1 ppbv, sometimes even greater than 10 ppbv. Again, the reductions in central and eastern CN are higher than that in western CN. These results are also partly related to the background mixing ratios. The decrease in JK ranges from 0.1 to 5 ppbv throughout the year, without obvious fluctuation.

With regard to the relative differences between the original and improved cases, the results seem slightly different, as shown in Fig. S1 in the Supplement. Although the reduction sequence is winter > autumn > spring > summer in general, which is very similar to the results above, the regional differences are no longer distinct. In winter, the mixing ratios of SO_2 decrease more than 50 % in most regions of EU and NA but no more than 50 % in central and eastern CN. In contrast, the reductions are very small in EU, NA, and JK in summer. However, the decreases exceed 10 % in CN and even 50 % in some regions (e.g., Shanxi, Hebei, Zhejiang, and Fujian provinces).

Such enhancement of the oxidation capacity can also be reflected in the net chemical loss rate of SO_2. Figure S2 shows the ratio of the net chemical loss rates between the improved and original simulations. The net chemical loss rate increases in most parts of the world (ratios > 1). The seasonal differences in the ratios are winter > autumn > spring > summer, which is still similar to the results above. The ratios in NA and JK are all more than 20 times greater and even above 100 times higher in some regions. Those in EU are more than 20 times greater in winter but less than 10 times higher in summer. The multiples in western CN are all more than 20 times greater and even more than 100 times greater in some regions, which are much higher than those in eastern CN, which are only less than 10 times greater.

3.3 Comparison between the simulated and observed SO_2 concentrations

The regional annual average mixing ratios between the simulated and *observed* SO_2 are summarized in Table 3. At the same time, scatterplots of SO_2 over various sites in the four monitoring networks are also shown in Fig. S3. Clearly, the effect of detailed aqueous-phase chemistry on the improvement in the SO_2 simulation is remarkable. The annual average mixing ratios in the original case are 4.3, 1.5, 2.0, and

Table 3. Comparison of regional annual average values among the observed, original-simulated, and improved-simulated SO_2 mixing ratios (ppbv) in EU, USA, CN, and JK in 2015. The observed mixing ratios are calculated by averaging the data from all monitoring stations of various measurement networks. The simulated mixing ratios are calculated by averaging the data from all the grids where the monitoring stations are located.

Region	Monitoring network	Obs	Ori	Imp
EU	EMEP*	0.38	2.0	1.0
US	EPA	1.1	2.7	1.6
CN	CNEMC*	10	30	23
JK	EANET	0.54	1.4	0.78

* The original units of EMEP and CNEMC are in micrograms of sulfur per cubic meter (hereafter $\mu g\,S\,m^{-3}$) and micrograms per cubic meter (hereafter $\mu g\,m^{-3}$), respectively. To facilitate comparison, these two units are converted to ppbv. Units conversion is as follows: $1\,mol\,mol_{air}^{-1} = 1\times10^9\,ppbv = \frac{64\times10^6 P_{air}}{RT_{air}}\,\mu g\,m^{-3} = \frac{32\times10^6 P_{air}}{RT_{air}}\,\mu g\,S\,m^{-3}$. The values of 64 and 32 are molar masses of SO_2 and S, respectively. The value of 10^6 is the unit conversion coefficient between grams (hereafter g) and micrograms (hereafter µg). $R = 8.314\,J\,mol^{-1}\,K^{-1}$ is the ideal gas constant. T_{air} (288 K used here) is atmospheric temperature in K. P_{air} (1.013×10^5 Pa used here) is atmospheric pressure in Pascal (hereafter Pa). The same applies below.

1.6 times overestimated in EU, USA, CN, and JK, respectively. After incorporating the detailed aqueous-phase chemistry, these values are reduced by 46 %, 41 %, 22 %, and 43 %, respectively. The slopes of the linear fitting lines are all close to or even approximately equal to 1 in EU, USA, and JK.

The comparison between the simulated and observed monthly average mixing ratios of SO_2 in the four monitoring networks is shown in Fig. 4. The relative differences between the original and improved simulations are also shown in Fig. S4. According to these two figures, compared with the observations, the original simulation is generally overestimated in all regions, especially in winter. Coupling the detailed in-cloud aqueous-phase chemical mechanisms greatly improves the simulation of SO_2. In EU, aqueous-phase reactions significantly improve the simulation of SO_2 from October to February. The simulated mixing ratios decrease by more than 60 % from the original case to the improved case and even by more than 75 % in December. The improved mixing ratios for 6 months are within the standard deviation of observations. The results in the USA are even better than those in EU. The mixing ratios of SO_2 decrease more in winter, spring, and autumn (−30 % to −70 %) than in summer. All improved mixing ratios are within the standard deviation of observations. Although the absolute reduction in SO_2 over CN is the greatest, the relative improvement in CN is the least due to the excessively high original mixing ratios of SO_2. None of the simulated mixing ratios decrease by more than 40 %. None of the improved mixing ratios are within the standard deviation of observations. The aqueous-phase reactions also greatly improve the simulation in JK. The relative differences in the four seasons are all close (approximately −30 % to −60 %). Almost all the improved mixing ratios are also within the standard deviation of observations.

Overall, the overestimation in winter is more serious than that in summer. At the same time, the improvement from adding aqueous-phase chemistry is much greater in winter than in summer, especially in EU and USA. These results indicate the importance of incorporating detailed aqueous-phase chemistry in winter and are highly consistent with the results of some existing studies (Shao et al., 2019; Ma et al., 2018; Huang et al., 2019). Such seasonal differences may be related to the ambient temperature, humidity, and especially sunlight. In summer, both the temperature and sunlight are sufficient to generate a high concentration of •OH (Lakey et al., 2016). Therefore, gas-phase oxidation is strong and dominant (Cheng et al., 2016). However, due to the weak sunlight in winter, the gas-phase concentration of •OH is 2 or 3 orders of magnitude less than that in summer. In addition, the rate constant is also less than one-third to one-half of that in summer, owing to the decrease in temperature. Therefore, the gas-phase photochemical oxidation of SO_2 induced by •OH is sharply weakened. These changes indicate the greatly increased importance of aqueous-phase reactions (Elser et al., 2016; Ervens, 2015; Harris et al., 2013; Huang et al., 2018). At the same time, higher humidity and more cloud coverage can provide a more sufficient aqueous environment, which is also beneficial to improve the performance of aqueous-phase reactions, such as those that occur during winter in EU and USA and summer in EA.

4 Contributions of different aqueous-phase chemical mechanisms to the oxidation of SO_2

On the basis of the above analysis of the overall detailed aqueous-phase chemistry, it is necessary to discuss the contributions of different aqueous-phase chemical mechanisms in detail. Cases for four different mechanisms are performed with the corresponding reactions in Tables 1 and 2. See Table S1 for details about the configuration of individual cases. Given the fact that the HO_x chemistry involves most of the critical radicals in aqueous-phase chemistry, the cases of Fe, N, and carbonate chemistry also include the HO_x chemistry. The individual contribution of Fe, N, or carbonate chemistry is compared with the HO_x chemistry case alone.

Figure 5 shows the effects of HO_x chemistry, Fe chemistry, N chemistry, and carbonate chemistry on surface SO_2 (case 3∼6 – case 1). Remarkable differences are clearly seen among these four mechanisms. On the one hand, generally speaking, the contributions from both HO_x chemistry and Fe chemistry to the oxidation of SO_2 are significant. Nonetheless, the seasonal and regional distribution properties of these two chemical mechanisms are obviously different. For HO_x chemistry, the mixing ratios of SO_2 decrease in most parts of the world, and the seasonal differences

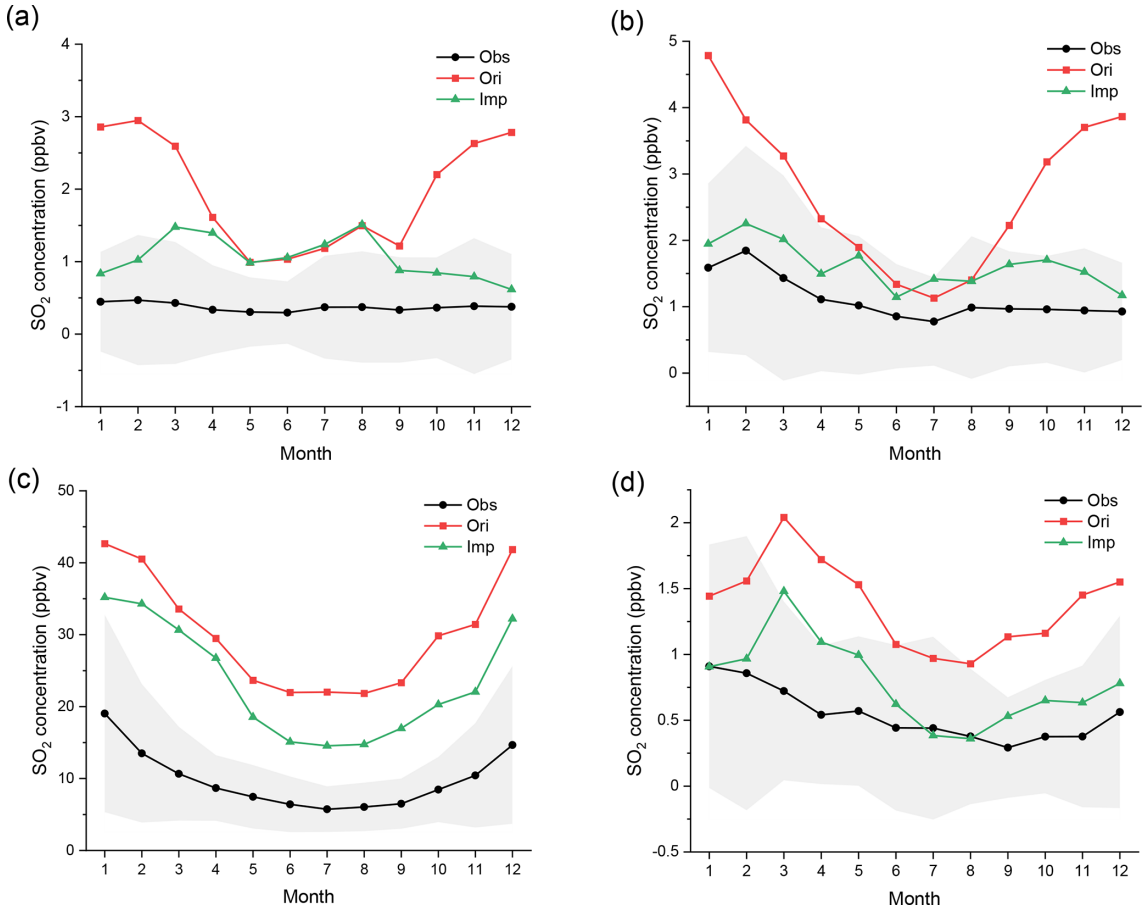

Figure 4. Regional monthly average mixing ratios (ppbv) of SO_2 in EU, USA, CN, and JK in 2015. The black, red, and green lines represent the observed, original-simulated, and improved-simulated mixing ratios, respectively. The gray areas represent the standard deviation of observed mixing ratios. The corresponding monitoring networks are **(a)** EMEP, **(b)** EPA, **(c)** CNEMC, and **(d)** EANET.

are very small. The reductions generally range from 0.01 to 0.1 ppbv over the ocean and 0.1–5 ppbv over land. With regard to Fe chemistry, however, the reduction in SO_2 is mostly concentrated on land only, especially in the Northern Hemisphere. The seasonal properties of the reductions are nearly the same as those described in Sect. 3.2. On the other hand, these two chemical mechanisms contribute much more than N chemistry to the oxidation of SO_2. The decrease in SO_2 exceeds 1 ppbv in many regions of Asia, EU, and NA due to the effects of Fe chemistry or HO_x chemistry. However, the contribution of N chemistry almost never exceeds 1 ppbv. Such a great disparity may be related to the level of Fe concentrations and pH values in cloud water, which are discussed in Sect. 5. With regard to carbonate chemistry, however, it is difficult to see consistent change in either spatial or temporal SO_2 distribution. The mixing ratios of SO_2 decrease in some places and seasons but increase in other places and seasons. Moreover, all the changes are very small, within ± 0.1 ppbv. Therefore, carbonate chemistry has no significant effect on the oxidation of SO_2.

The contributions of the different chemical mechanisms discussed above can also be seen from the relative differences, as shown in Fig. S5. HO_x chemistry contributes the most over the ocean in the Southern Hemisphere. At the same time, Fe chemistry contributes the most over land in the Northern Hemisphere. The mixing ratios of SO_2 decrease by more than 50 % in both mechanisms. Furthermore, note that, although the contribution of carbonate chemistry is quite small, there is an evident decrease over the ocean in the Southern Hemisphere.

5 Factors affecting the capacity for SO_2 oxidation from aqueous-phase reactions

5.1 The concentration of soluble Fe

The concentrations of soluble $[Fe^{3+}]$ are all set to 5 µM in the improved case. Nevertheless, $[Fe^{3+}]$ varies greatly in different regions, seasons, and ambient conditions. For instance, $[Fe^{3+}]$ is generally no more than 0.1 µM under marine condi-

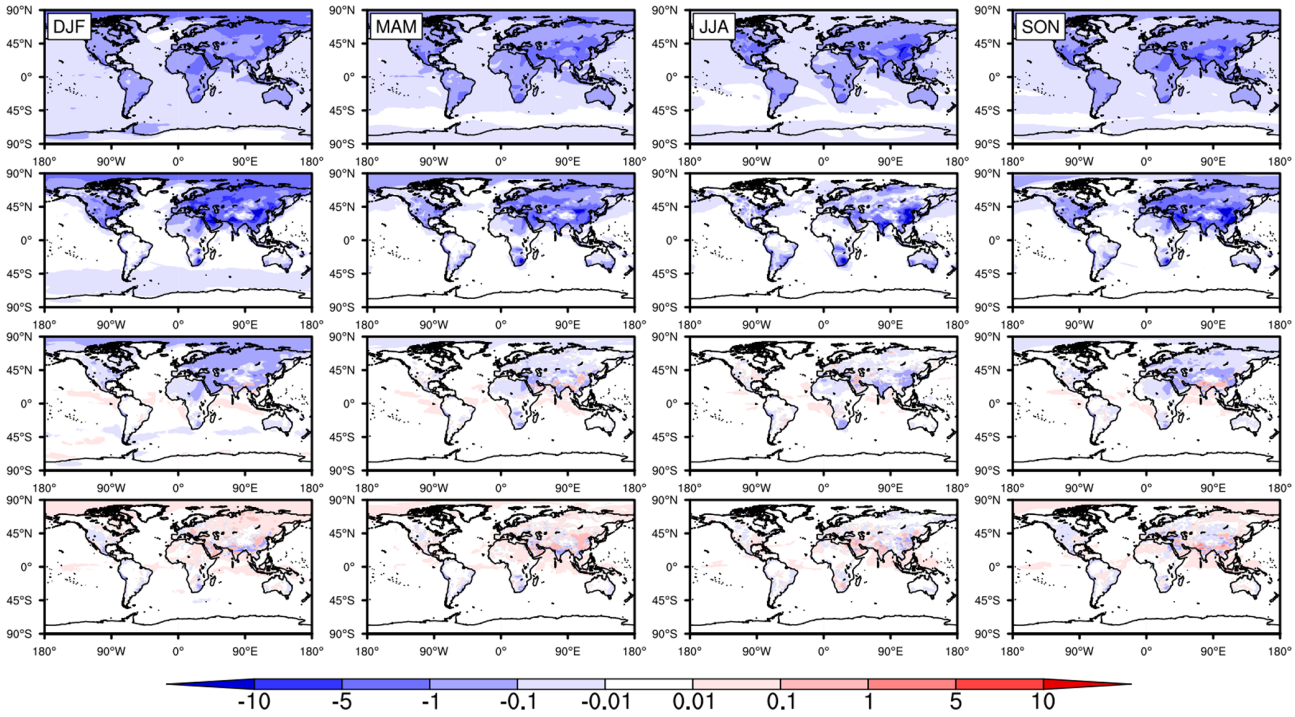

Figure 5. The differences in global seasonally averaged surface SO_2 mixing ratios (ppbv) in 2015 with the incorporation of HO_x chemistry, Fe chemistry, N chemistry, and carbonate chemistry individually from top to bottom, respectively.

tions and no more than 1 µM under remote continental conditions (Herrmann et al., 2000; Matthijsen et al., 1995; Deguillaume et al., 2005; Mao et al., 2013; Jacob, 2000; Shao et al., 2019; Li et al., 2017). In many polluted cities, $[Fe^{3+}]$ is much higher than that in remote regions, usually ranging from 5 to 20 µM and sometimes even exceeding 100 µM (Matthijsen et al., 1995; Deguillaume et al., 2005; Herrmann et al., 2000; Mao et al., 2013; Jacob, 2000; Li et al., 2017). Therefore, in this study, four other levels of initial $[Fe^{3+}]$ (0.1, 1, 20, and 100 µM) are tested with the whole in-cloud aqueous-phase reactions to evaluate the influence of soluble Fe concentration on the capacity for SO_2 oxidation. The processing $[Fe^{3+}]$ in these sensitivity cases is identical to the improved case, except for the differences in Fe^{3+} concentrations. All the levels of $[Fe^{3+}]$ are based on the reported values above. See Table S1 for details.

The regional monthly average mixing ratios of SO_2 in four regions are shown in Fig. 6. In all four regions, the simulated SO_2 first still increases in summer when initial $[Fe^{3+}]$ is 0.1 µM and then decreases considerably when initial $[Fe^{3+}]$ increases from 0.1 to 5 µM but declines only slightly when initial $[Fe^{3+}]$ increases to 20 µM. The two lines of $[Fe] = 20$ µM and $[Fe] = 100$ µM almost overlap and cannot be distinguished clearly in EU, USA, and JK. Only in CN do the mixing ratios of SO_2 further decrease obviously when initial $[Fe^{3+}]$ increases from 5 to 100 µM. There are many steel and coal factories and power plants in CN. These results imply that there may be a strong correlation between high emissions of SO_2 and iron, and that the concentrations of Fe in CN may be higher than those in other regions.

Such an effect on the capacity for SO_2 oxidation by $[Fe^{3+}]$ chemistry can also be seen in Fig. S6. The capacity for SO_2 oxidation is enhanced with increasing $[Fe^{3+}]$ on the whole. When initial $[Fe^{3+}]$ is only 0.1 µM, the effect of Fe chemistry is still quite weak. The effect is rapidly enhanced when initial $[Fe^{3+}]$ increases from 0.1 to 5 µM. However, such enhancement becomes markedly less when initial $[Fe^{3+}]$ is greater than 20 µM. The mixing ratios of SO_2 is almost unchanged when initial $[Fe^{3+}]$ increases to 100 µM. This result indicates that the effect of increasing $[Fe^{3+}]$ on the capacity for SO_2 oxidation has a threshold. Too much $[Fe^{3+}]$ will not further facilitate the oxidation of SO_2. The reason for such a limitation is discussed below.

In any case, a higher concentration of soluble Fe results in an improvement in the SO_2 simulation compared to the observations.

5.2 The pH value

As mentioned in the Introduction, the pH value in cloud water is a key parameter for aqueous-phase chemistry, which could directly affect ionization equilibria and gas–aqueous mass transfer processes. There are expressions for the rate constants of several aqueous-phase reactions, and some expressions include pH values directly. Therefore, the pH value could affect the various aqueous-phase reaction rates, espe-

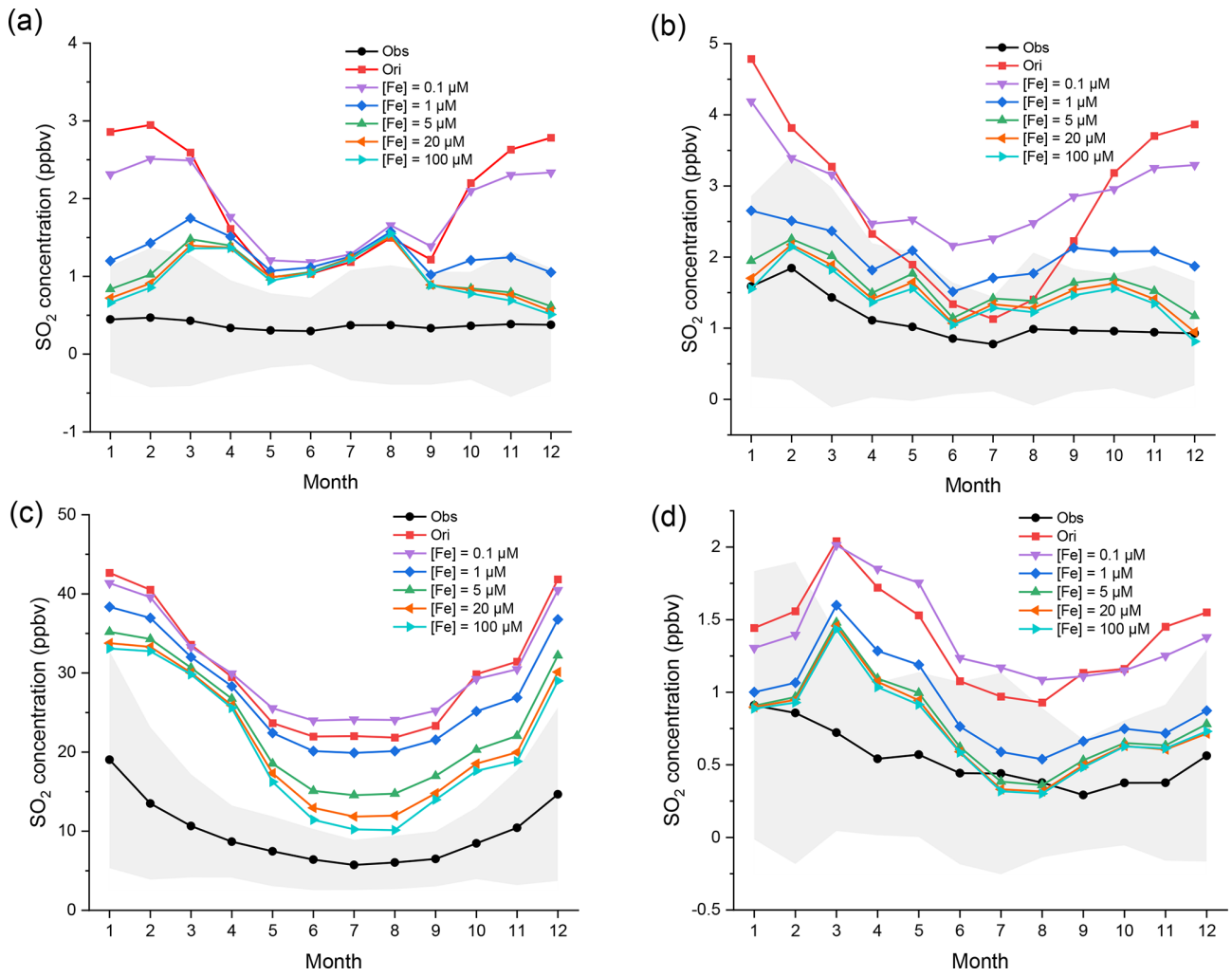

Figure 6. Regional monthly average mixing ratios (ppbv) of SO_2 in EU, USA, CN, and JK in 2015. The black and red lines represent the observed and original-simulated mixing ratios of SO_2, respectively. Other lines represent SO_2 mixing ratios with different soluble [Fe^{3+}]. [Fe^{3+}], from top to bottom, is 0.1, 1, and 5 (i.e., the improved case) and 20 and 100 µM, respectively. The gray areas represent the standard deviation of observed mixing ratios. The corresponding monitoring networks are **(a)** EMEP, **(b)** EPA, **(c)** CNEMC, and **(d)** EANET.

cially that of N chemistry (Shao et al., 2019; Li et al., 2017; Cheng et al., 2016; He et al., 2018; He and He, 2020). Therefore, it is necessary to discuss the influence of the variation in the pH value on the capacity for SO_2 oxidation. In this study, there are four sets of pH values (i.e., 3, 4, 5, and 6) prescribed in the following sensitivity tests (Table S1). All the pH values are referenced from previous studies (Herrmann et al., 2000; Matthijsen et al., 1995; Shao et al., 2019; Guo et al., 2017; Cheng et al., 2016). [Fe^{3+}] is set to 5 µM. However, it is difficult to see obvious differences among these four pH levels in all seasons. Only a small decrease in SO_2 can be seen in most regions from pH 3 to 4. The reduction in SO_2 is almost the same from pH 4 to 6. This result indicates that the effect of increasing the pH value on the capacity for SO_2 oxidation is limited.

The global distributions of SO_2 in different seasons, shown in Fig. S7, have similar features. Although the capacity for SO_2 oxidation increases to some extent from pH 3 to 4 in all four regions, the changes from pH 4 to 6 are very small.

Notwithstanding, a higher pH value doubtless enhances the capacity for SO_2 oxidation and results in simulated values that are closer to the observations, which is similar to the influence of the soluble Fe concentration (Shi et al., 2019; Shao et al., 2019; Li et al., 2017; Cheng et al., 2016).

It seems that the influence of the pH value on the aqueous-phase chemistry is much weaker than that of the soluble Fe concentration. When further discussing the effect of the pH value on N chemistry, HO_x chemistry, or Fe chemistry individually, however, the situation is quite different, as shown in Table S1 and Figs. S8–S10. When the pH increases from 3 to 6, the capacity for SO_2 oxidation from N chem-

istry and HO_x chemistry is evidently enhanced at all times. When the pH is 6, the oxidation capacity from N chemistry and HO_x chemistry becomes almost as strong as that from Fe chemistry with a high concentration of soluble Fe. This indicates that the capacity for SO_2 oxidation from N chemistry and HO_x chemistry is greatly affected by the pH value (Wang et al., 2020; Cheng et al., 2016; He et al., 2018; L. Li et al., 2018; He and He, 2020). In contrast, the capacity for SO_2 oxidation from Fe chemistry is the opposite. When $[Fe^{3+}]$ is set at the default medium level (5 µM), regardless of the pH, there are no remarkable changes in the SO_2 mixing ratios, and the capacity for SO_2 oxidation from Fe chemistry is nearly the same, especially when the pH ranges from 4 to 6. This indicates that the Fe chemistry is not significantly affected by pH.

These results explain well why the contribution of N chemistry is much smaller than that of Fe chemistry and HO_x chemistry in Sect. 4. According to the simulation, the pH value in cloud water is generally in the range of 3–5. This pH range is highly consistent with those in previous studies (Herrmann et al., 2000; Matthijsen et al., 1995; Shao et al., 2019; Guo et al., 2017; Cheng et al., 2016). As seen in Fig. 5, the capacity for SO_2 oxidation from N chemistry is between pH 4 and 5, which is still not strong enough. Consequently, the capacity for SO_2 oxidation from N chemistry is largely limited by the relatively low pH values in cloud water.

As analyzed in the sections above, it is worth noting that, regardless of the high soluble Fe concentration or high pH value for different chemical mechanisms, the reduction in SO_2 always seems to reach a very similar limitation, and the global distribution and regional monthly average mixing ratios are also almost the same. This is not only related to soluble Fe concentration, pH value, or the chemical properties of various mechanisms themselves but is also derived from the exhaustion of SO_2(aq) by detailed aqueous-phase chemistry in a finite cloud. The aqueous-phase chemistry cannot affect regions without clouds because the total SO_2 is calculated by weighted averages of cloudy and non-cloudy conditions, according to F_{cld}. The overestimated SO_2 is sometimes caused by a shortage of clouds, especially in CN. Therefore, only more cloud coverage or lower emissions may further reduce the overestimation.

Consequently, it is easy to conclude that the oxidation capacity of Fe chemistry and HO_x chemistry is much higher than that of N chemistry when the pH is less than 5, but evaluating their relative importance at high pH is difficult. The cloud content and substrate concentration become the limiting factors. Therefore, a comprehensive investigation of cloud pH in different seasons and at different places is urgently needed.

5.3 Discussion and uncertainty analysis

Recent studies show that hydroxymethanesulfonate (HMS), formed by aqueous-phase reactions of dissolved HCHO and SO_2, is an abundant organosulfur compound in aerosols during winter haze episodes and suggest that aqueous clouds act as the major medium for HMS chemistry (Moch et al., 2020; Song et al., 2021). Therefore, it is necessary to further investigate the influence of this organic chemistry on the in-cloud aqueous-phase chemistry system in CESM2. We tried to incorporate 10 aqueous-phase organic species and 60 related reactions, including the reactions related to CH_3OH, HCHO, CH_3OOH, and HMS, as shown in Table S2a and b. We conducted additional simulations for testing the contribution from this organic chemistry. As shown in Fig. S11, incorporating this organic chemistry has a minor effect on SO_2 concentrations, similar to that of carbonate chemistry.

In addition to the soluble Fe concentration and pH value discussed above, there are some other factors that may also affect the capacity for SO_2 oxidation and increase the uncertainty of the simulation. First, the simulation of variables related to cloud properties (such as LWC, F_{cld}, and r) directly determines the contribution of aqueous-phase chemistry. However, the simulation of these variables is also one of the greatest uncertainties (Zhang et al., 2019; Faloona, 2009). In addition, the initial valence of soluble Fe and the proportion of various valences are related to the capacity of Fe chemistry. The higher the proportion of Fe^{3+}, the stronger the atmospheric oxidizability and the more helpful it is for the oxidation of SO_2 (Jacob, 2000; Deguillaume et al., 2005; Huang et al., 2014; Alexander et al., 2009). Moreover, the emissions and solubility of Fe vary greatly in different regions. For instance, the total concentration of atmospheric Fe is generally measured in the range of 1–1000 $ng\,m_{air}^{-3}$, and the solubility of elemental Fe varies from less than 1 % to 10 % (Cwiertny et al., 2008; Hsu et al., 2010, 2013; Sedwick et al., 2007; Sholkovitz et al., 2009; Heal et al., 2005; Ingall et al., 2018; Mao et al., 2013; Itahashi et al., 2018; Shelley et al., 2018; Mcdaniel et al., 2019; Conway et al., 2019; Shi et al., 2020; Myriokefalitakis et al., 2018; Wang et al., 2015). Meanwhile, the simulated LWC usually ranges from 10^{-8} to 10^{-5} $L_{water}\,L_{air}^{-1}$ in CESM2 and other model studies (Herrmann et al., 2000, 2015; Jacob, 1986; Matthijsen et al., 1995; J. Liu et al., 2012). In addition, F_{cld} should also be considered. Therefore, the concentration of soluble Fe can be calculated in a range from less than 10^{-3} to 10^{3} µM, involving great uncertainties. It is also the reason why the dust aerosol is simulated but not coupled with soluble Fe in this study. At the same time, the proportions of aerosols containing sulfate, nitrate, and ammonium in the aqueous phase could directly affect the pH of cloud water. The simulated pH value of cloud water itself is one of the sources of uncertainty (Shi et al., 2019; Xue et al., 2016). Finally, some sources of kinetic parameters for the aqueous-phase reactions are outdated. They may also not be accurate enough because measurement conditions in the laboratory are different from the conditions of the real atmosphere. These issues influence the accuracy of the reaction rates and increase the uncertainty of the simulation.

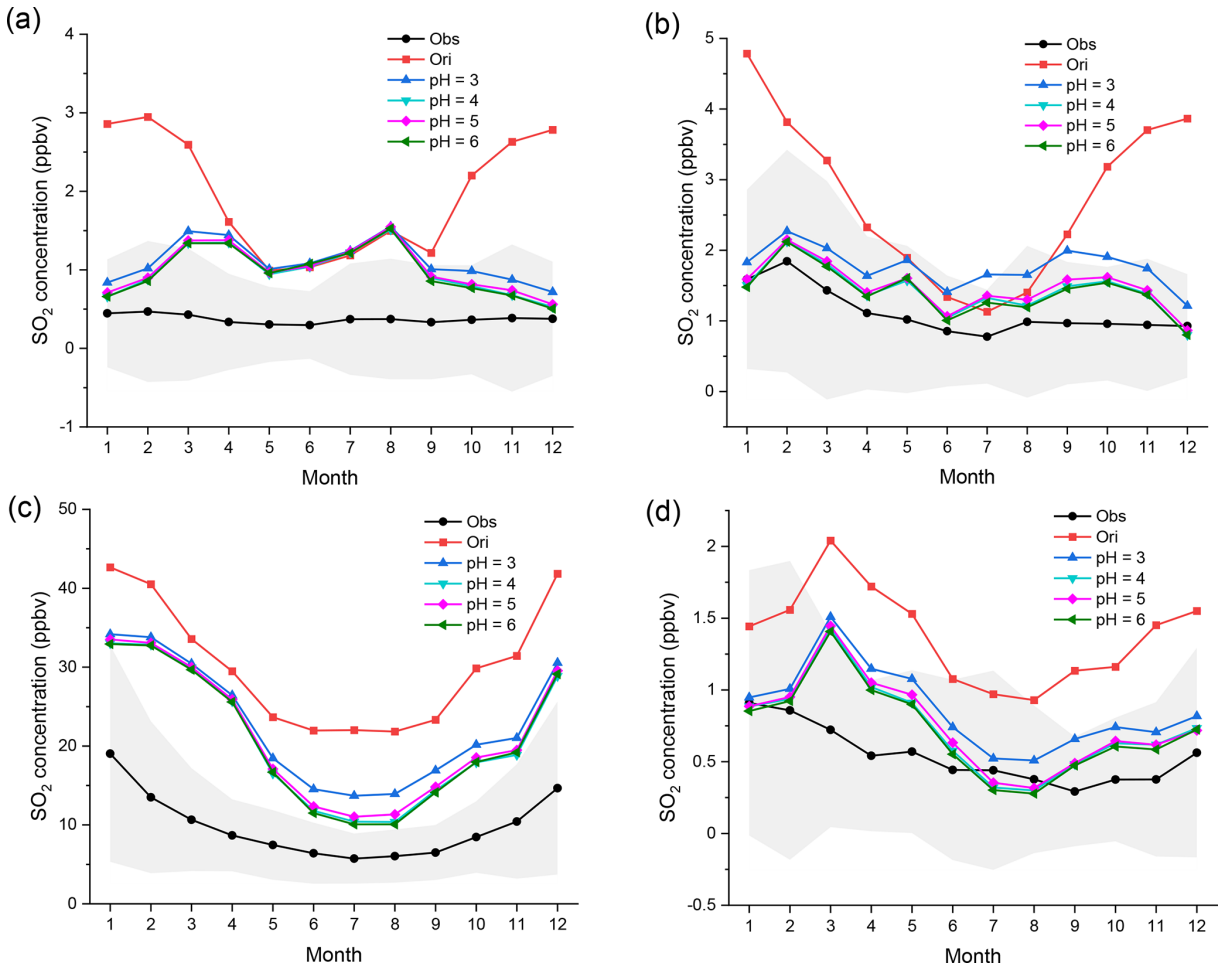

Figure 7. Regional monthly average mixing ratios (ppbv) of SO_2 in EU, USA, CN, and JK in 2015. The black and red lines represent the observed and original-simulated mixing ratios of SO_2, respectively. Other lines represent SO_2 mixing ratios at different pH values. The pH values, from top to bottom, are 3, 4, 5, and 6, respectively. $[Fe^{3+}]$ is set to 5 µM. The gray areas represent the standard deviation of observed mixing ratios. The corresponding monitoring networks are **(a)** EMEP, **(b)** EPA, **(c)** CNEMC, and **(d)** EANET.

In addition, there are factors that affect the performance of the simulation to a certain degree. First, an accurate emission inventory is the premise for improving the simulation (Im et al., 2018; De Meij et al., 2006; Liu et al., 2018; Buchard et al., 2014). The data sources and resolutions of various emission types could affect the reliability of the inventory. For instance, regardless of how the parameters discussed above are optimized, the concentration of SO_2 in CN is always overestimated, which may be related to the uncertainties in emission inventories. The emissions of SO_2 in CN have decreased considerably in recent years, which may lead to biases in the simulations (Jo et al., 2020; Xie et al., 2016; Geng et al., 2019). Meanwhile, the meteorological data include information on the water content, wind, temperature, and pressure, which all influence the formation and movements of clouds. Therefore, the reliability of meteorological data is also related to the uncertainty of simulations with in-cloud chemistry (Bei et al., 2017; Liu et al., 2007). At the same time, the simulation of the SO_2 wet deposition process also involves great uncertainty. Furthermore, the selection of monitoring stations determines the quality of observational data. As a global model, CESM2 used in this study has a resolution that is still not fine enough to accurately simulate regions that are too remote or too close to pollution sources. The simulation of each grid can represent only the average level of a region. Therefore, the monitoring stations should also represent the average level of the region. Otherwise, the limitation of the model resolution also increases the deviation of the comparison with observations and the uncertainty of the simulations. Finally, there are slight numerical fluctuations during the calculation of the model itself, but the uncertainty from the fluctuations is very small and can be ignored, especially after the results are averaged.

6 Conclusions

To improve the global simulation of SO_2 in this study, we used CESM2 to evaluate the effects of detailed in-cloud aqueous-phase reaction mechanisms on the capacity for SO_2 oxidation. After the replacement of default simplified and parameterized aqueous-phase reactions with detailed in-cloud aqueous-phase reactions, the overestimation of surface SO_2 generally decreases significantly. The reductions vary in different regions and seasons. Most them are in the range of 0.1–10 ppbv, and some can be greater than 10 ppbv in some regions of CN. The net chemical loss rate of SO_2 also increases substantially. When compared with the observations, the simulated values that incorporate detailed aqueous-phase chemistry improve greatly, making the simulations much closer to the observations. The biases of annual average simulated mixing ratios decrease by 46 %, 41 %, 22 %, and 43 % in EU, USA, CN, and JK, respectively. The mixing ratio even decreases by approximately 70 % in winter in EU, which is very close to the observed value. The mixing ratios of SO_2 in CN are still highly overestimated, although they decrease considerably. Aqueous-phase chemistry contributes more in EU, USA, and JK than in CN, which may be related to cloud coverage and emissions.

The contribution of each aqueous-phase mechanism to the simulation of SO_2 also differs significantly. Fe chemistry and HO_x chemistry contribute more to the capacity for SO_2 oxidation than N chemistry. Carbonate chemistry has no significant effect on the oxidation of SO_2. Several factors could influence the capacity for SO_2 oxidation. Higher concentrations of soluble Fe and higher pH values could further enhance the oxidation capacity and improve the simulation of SO_2. In addition, the oxidation capacities from N chemistry and HO_x chemistry are strongly affected by pH values and increase rapidly with increasing pH. The oxidation capacity from Fe chemistry is almost unaffected by pH. Many other factors also affect the aqueous-phase chemistry and the simulation of SO_2. Regardless of which factor changes, there is still a limitation on the improvement in the simulations because of limited cloud coverage in the aqueous phase.

This study emphasizes the importance of aqueous-phase chemical mechanisms for SO_2 oxidation. These mechanisms are helpful to improve the simulation of SO_2 by CESM2, deepening the understanding of SO_2 oxidation and the formation of sulfate, $PM_{2.5}$, and even hazy days. A better simulation of SO_2 is a prerequisite for better representing sulfate, which further influences cloud microphysics, radiation transfer, and climate change.

However, some aspects still need to be further studied and improved in the future. For instance, there is a high degree of uncertainty in the concentration of soluble Fe owing to the dramatically large variation in the total atmospheric Fe content and Fe solubility in different regions. At the same time, there are few observational data or emission inventories of soluble Fe. Therefore, the contribution of Fe chemistry to the capacity for SO_2 oxidation is uncertain under different atmospheric conditions and difficult to evaluate accurately. Meanwhile, many variables and parameters related to the simulated clouds are also uncertain, such as LWC, F_{cld}, r, pH values in clouds, wet deposition processes, and proportions of inorganic aerosols in the aqueous phase. Therefore, it is urgently necessary to compare these variables with observational data if possible. Moreover, the effect of aqueous-phase chemistry on SO_2 at high altitude is not discussed in this study. These issues will be examined in our future work.

Code availability. The Community Earth System Model 2 (CESM2) developed by the National Center for Atmospheric Research can be downloaded (https://www.cesm.ucar.edu/models/cesm2/, CESM Working Groups of National Center for Atmospheric Research, 2020a). All codes used to generate the results of this study are available from the authors upon request.

Data availability. The CMIP6 emission data sets analyzed during the current study are available at https://svn-ccsm-inputdata.cgd.ucar.edu/trunk/inputdata/atm/cam/chem/ (CESM Working Groups of National Center for Atmospheric Research, 2020b). The MERRA-2 meteorological offline data are publicly available from https://rda.ucar.edu/datasets/ds313.3/ (Data Engineering and Curation Section of the Computational and Information Systems Laboratory at the National Center for Atmospheric Research, 2020).

Supplement. The supplement related to this article is available online at: https://doi.org/10.5194/acp-21-16093-2021-supplement.

Author contributions. WG revised and operated the model, processed and analyzed the results, and wrote the paper. JL guided WG's research and helped to revise the paper. KY and JX taught WG the installation and usage of CESM2. YZ and XH provided suggestions. JM, XW, YW, JH, ZZ, XW, and ST provided funding support.

Competing interests. The contact author has declared that neither they nor their co-authors have any competing interests.

Disclaimer. Publisher's note: Copernicus Publications remains neutral with regard to jurisdictional claims in published maps and institutional affiliations.

Acknowledgements. We are very grateful to the two referees for their valuable comments on our paper. We thank Songlin Xiang, Huazhen Liu, Jingcheng Zhou, Yuqing Wang, and Qiong Yang for their help and suggestions on model installation, data collection, and result processing.

We thank engineers Zhen Zhang and Ge Peng for their maintenance of the model platform.

This work has been supported by funding from the National Natural Science Foundation of China (grant nos. 42077196 and 41821005) and the Newton Advanced Fellowship (grant no. NAFR2180103).

Financial support. This work has been supported by funding from the National Natural Science Foundation of China (grant nos. 42077196 and 41821005) and the Newton Advanced Fellowship (grant no. NAFR2180103).

Review statement. This paper was edited by Thomas von Clarmann and reviewed by two anonymous referees.

References

Acid Deposition Monitoring Network in East Asia: Data Report, Acid Deposition Monitoring Network in East Asia [data set], available at: https://monitoring.eanet.asia/document/public/index, last access: 2 November 2020.

Adams, G. E. and Boag, J. W.: Spectroscopic studies of reactions of the OH radical, P. Chem. Soc. London, 1, 112–118, 1964.

Alexander, B., Park, R. J., Jacob, D. J., and Gong, S.: Transition metal-catalyzed oxidation of atmospheric sulfur: Global implications for the sulfur budget, J. Geophys. Res., 114, D02309, https://doi.org/10.1029/2008jd010486, 2009.

Amels, P., Elias, H., Götz, U., Steinges, U., and Wannowius, K. J.: Kinetic investigation of the stability of peroxonitric acid and of its reaction with sulfur(IV) in aqueous solution, in: Heterogeneous and Liquid Phase Processes, edited by: Warneck, P., Transport and Chemical Transformation in Pollutants in the Troposphere, Springer, Berlin, 77–88, 1996.

Au Yang, D., Bardoux, G., Assayag, N., Laskar, C., Widory, D., and Cartigny, P.: Atmospheric SO_2 oxidation by NO_2 plays no role in the mass independent sulfur isotope fractionation of urban aerosols, Atmos. Environ., 193, 109–117, https://doi.org/10.1016/j.atmosenv.2018.09.007, 2018.

Bao, Z. C. and Barker, J. R.: Temperature and ionic strength effects on some reactions involving sulfate radical [SO_4^-(aq)], J. Phys. Chem.-US, 100, 9780–9787, 1996.

Bataineh, H., Pestovsky, O., and Bakac, A.: pH-induced mechanistic changeover from hydroxyl radicals to iron(IV) in the Fenton reaction, Chem. Sci., 3, 1594–1599, https://doi.org/10.1039/c2sc20099f, 2012.

Behar, D., Czapski, G., and Duchovny, I.: Carbonate Radical in Flash Photolysis and Pulse Radiolysis of Aqueous Carbonate Solutions, J. Phys. Chem.-US, 74, 2206–2210, 1970.

Bei, N., Wu, J., Elser, M., Feng, T., Cao, J., El-Haddad, I., Li, X., Huang, R., Li, Z., Long, X., Xing, L., Zhao, S., Tie, X., Prévôt, A. S. H., and Li, G.: Impacts of meteorological uncertainties on the haze formation in Beijing–Tianjin–Hebei (BTH) during wintertime: a case study, Atmos. Chem. Phys., 17, 14579–14591, https://doi.org/10.5194/acp-17-14579-2017, 2017.

Beilke, S. and Gravenhorst, G.: Heterogeneous SO_2-oxidation in the droplet phase, Atmos. Environ., 12, 231–239, 1978.

Bell, N., Koch, D., and Shindell, D. T.: Impacts of chemistry-aerosol coupling on tropospheric ozone and sulfate simulations in a general circulation model, J. Geophys. Res.-Atmos., 110, D14305, https://doi.org/10.1029/2004jd005538, 2005.

Benkelberg, H. J. and Warneck, P.: Photodecomposition of Iron(III) Hydroxo and Sulfato Complexes in Aqueous-Solution – Wavelength Dependence of OH and SO_4^- Quantum Yields, J. Phys. Chem.-US, 99, 5214–5221, https://doi.org/10.1021/j100014a049, 1995.

Betterton, E. A. and Hoffmann, M. R.: Oxidation of Aqueous SO_2 by Peroxymonosulfate, J. Phys. Chem.-US, 92, 5962–5965, https://doi.org/10.1021/j100332a025, 1988.

Bielski, B. H. J., Cabelli, D. E., Arudi, R. L., and Ross, A. B.: Reactivity of HO_2/O_2^- Radicals in Aqueous-Solution, J. Phys. Chem. Ref. Data, 14, 1041–1100, https://doi.org/10.1063/1.555739, 1985.

Bongartz, A., Schweighoefer, S., Roose, C., and Schurath, U.: The Mass Accommodation Coefficient of Ammonia on Water, J. Atmos. Chem., 20, 35–58, https://doi.org/10.1007/Bf01099917, 1995.

Boniface, J., Shi, Q., Li, Y. Q., Cheung, J. L., Rattigan, O. V., Davidovits, P., Worsnop, D. R., Jayne, J. T., and Kolb, C. E.: Uptake of gas-phase SO_2, H_2S, and CO_2 by aqueous solutions, J. Phys. Chem. A, 104, 7502–7510, 2000.

Brandt, C. and Vaneldik, R.: Transition-Metal-Catalyzed Oxidation of Sulfur(IV) Oxides – Atmospheric-Relevant Processes and Mechanisms, Chem. Rev., 95, 119–190, https://doi.org/10.1021/cr00033a006, 1995.

Bray, W. C. and Gorin, M. H.: Ferryl ion, a compound of tetravalent iron, J. Am. Chem. Soc., 54, 2124–2125, https://doi.org/10.1021/ja01344a505, 1932.

Buchard, V., da Silva, A. M., Colarco, P., Krotkov, N., Dickerson, R. R., Stehr, J. W., Mount, G., Spinei, E., Arkinson, H. L., and He, H.: Evaluation of GEOS-5 sulfur dioxide simulations during the Frostburg, MD 2010 field campaign, Atmos. Chem. Phys., 14, 1929–1941, https://doi.org/10.5194/acp-14-1929-2014, 2014.

Buhler, R. E., Staehelin, J., and Hoigne, J.: Ozone Decomposition in Water Studied by Pulse-Radiolysis .1. HO_2/O_2^- and HO_3/O_3^- as Intermediates, J. Phys. Chem.-US, 88, 2560–2564, 1984.

Buxton, G. V., Wood, N. D., and Dyster, S.: Ionization-Constants Of OH and HO_2 in Aqueous-Solution up to 200 °C. A Pulse–Radiolysis Study, J. Chem. Soc. Faraday T., 1, 1113–1121, https://doi.org/10.1039/f19888401113, 1988a.

Buxton, G. V., Greenstock, C. L., Helman, W. P., and Ross, A. B.: Critical-Review of Rate Constants for Reactions of Hydrated Electrons, Hydrogen-Atoms and Hydroxyl Radicals (OH/O_2^-) in Aqueous-Solution, J. Phys. Chem. Ref. Data, 17, 513–886, https://doi.org/10.1063/1.555805, 1988b.

Buxton, G. V., Malone, T. N., and Salmon, G. A.: Pulse radiolysis study of the reaction of SO_5^- with HO_2, J. Chem. Soc. Faraday T., 92, 1287–1289, https://doi.org/10.1039/ft9969201287, 1996a.

Buxton, G. V., McGowan, S., Salmon, G. A., Williams, J. E., and Woods, N. D.: A study of the spectra and reactivity of oxysulphur-radical anions involved in the chain oxidation of S(IV): A pulse and gamma-radiolysis study, Atmos. Environ., 30, 2483–2493, https://doi.org/10.1016/1352-2310(95)00473-4, 1996b.

Buxton, G. V., Malone, T. N., and Salmon, G. A.: Reaction of SO_4^- with Fe^{2+}, Mn^{2+} and Cu^{2+} in aqueous solution, J. Chem. Soc. Faraday T., 93, 2893–2897, https://doi.org/10.1039/a701472d, 1997.

Buxton, G. V., Barlow, S., McGowan, S., Salmon, G. A., and Williams, J. E.: The reaction of the SO_3^- radical with Fe(II) in acidic aqueous solution – A pulse radiolysis study, Phys. Chem. Chem. Phys., 1, 3111–3115, 1999.

CESM Working Groups of National Center for Atmospheric Research (NCAR): Community Earth System Model, available at: https://svn-ccsm-inputdata.cgd.ucar.edu/trunk/inputdata/atm/cam/chem/, CESM Working Groups of National Center for Atmospheric Research (NCAR) [code], last access: 16 December 2020.

CESM Working Groups of National Center for Atmospheric Research (NCAR): Title: Revision 36285: /trunk/inputdata/atm/cam/chem, available at: CESM Working Groups of National Center for Atmospheric Research, CESM Working Groups of National Center for Atmospheric Research (NCAR) [data set], last access: 31 December 2020.

Chameides, W. L.: The photochemistry of a Remote Marine Straaatiform Cloud, J. Geophys. Res., 89, 4739–4755, 1984.

Chen, Y., Luo, X. S., Zhao, Z., Chen, Q., Wu, D., Sun, X., Wu, L., and Jin, L.: Summer-winter differences of $PM_{2.5}$ toxicity to human alveolar epithelial cells (A549) and the roles of transition metals, Ecotox. Environ. Safe., 165, 505–509, https://doi.org/10.1016/j.ecoenv.2018.09.034, 2018.

Cheng, Y. F., Zheng, G. J., Wei, C., Mu, Q., Zheng, B., Wang, Z. B., Gao, M., Zhang, Q., He, K. B., Carmichael, G., Poschl, U., and Su, H.: Reactive nitrogen chemistry in aerosol water as a source of sulfate during haze events in China, Science Advances, 2, 1–11, ARTN e1601530 https://doi.org/10.1126/sciadv.1601530, 2016.

Chin, M. and Wine, P. H.: A temperature-dependent competitive kinetics study of the aqueousphase reactions of OH radicals with formate, formic acid, acetate, acetic acid and hydrated formaldehyde, in: Aquatic and Surface Photochemistry, edited by: Helz, G. R., Zepp, R. G., and Crosby, D. G., Lewis Publishers, Boca Raton, 85–96, 1994.

China National Environmental Monitoring Center: Historical data of air quality in China, China National Environmental Monitoring Center [data set], available at: https://quotsoft.net/air/, last access: 22 December 2020.

Christensen, H. and Sehested, K.: Pulse-Radiolysis at High-Temperatures and High-Pressures, Radiat. Phys. Chem., 18, 723–731, https://doi.org/10.1016/0146-5724(81)90195-3, 1981.

Christensen, H., Sehested, K., and Corfitzen, H.: Reactions of Hydroxyl Radicals with Hydrogen-Peroxide at Ambient and Elevated-Temperatures, J. Phys. Chem.-US, 86, 1588–1590, 1982.

Christensen, H., Sehested, K., and Bjergbakke, E.: Radiolysis of reactor water: Reaction of hydroxyl radicals with superoxide (O_2^-), Water Chemistry of Nuclear Reactor Systems, 5, 141–144, 1989.

Clegg, S. L. and Brimblecombe, P.: Solubility of volatile electolytes in multicomponent solutions with atmospheric applications, ACS Sym. Ser., 416, 58–73, 1990.

Conway, T. M., Hamilton, D. S., Shelley, R. U., Aguilar-Islas, A. M., Landing, W. M., Mahowald, N. M., and John, S. G.: Tracing and constraining anthropogenic aerosol iron fluxes to the North Atlantic Ocean using iron isotopes, Nat. Commun., 10, 1–10, https://doi.org/10.1038/s41467-019-10457-w, 2019.

Cwiertny, D. M., Baltrusaitis, J., Hunter, G. J., Laskin, A., Scherer, M. M., and Grassian, V. H.: Characterization and acid-mobilization study of iron-containing mineral dust source materials, J. Geophys. Res.-Atmos., 113, D05202, https://doi.org/10.1029/2007jd009332, 2008.

Damschen, D. E. and Martin, L. R.: Aqueous Aerosol Oxidation of Nitrous-Acid by O_2, O_3 and H_2O_2, Atmos. Environ., 17, 2005–2011, 1983.

Danabasoglu, G., Lamarque, J. F., Bacmeister, J., Bailey, D. A., DuVivier, A. K., Edwards, J., Emmons, L. K., Fasullo, J., Garcia, R., Gettelman, A., Hannay, C., Holland, M. M., Large, W. G., Lauritzen, P. H., Lawrence, D. M., Lenaerts, J. T. M., Lindsay, K., Lipscomb, W. H., Mills, M. J., Neale, R., Oleson, K. W., Otto-Bliesner, B., Phillips, A. S., Sacks, W., Tilmes, S., Kampenhout, L., Vertenstein, M., Bertini, A., Dennis, J., Deser, C., Fischer, C., Fox-Kemper, B., Kay, J. E., Kinnison, D., Kushner, P. J., Larson, V. E., Long, M. C., Mickelson, S., Moore, J. K., Nienhouse, E., Polvani, L., Rasch, P. J., and Strand, W. G.: The Community Earth System Model Version 2 (CESM2), J. Adv. Model. Earth Sy., 12, 1–35, https://doi.org/10.1029/2019ms001916, 2020.

Data Engineering and Curation Section of the Computational and Information Systems Laboratory at the National Center for Atmospheric Research (NCAR): MERRA2 Global Atmosphere Forcing Data, available at: https://rda.ucar.edu/datasets/ds313.3/, Data Engineering and Curation Section of the Computational and Information Systems Laboratory at the National Center for Atmospheric Research [data set], last access: 20 July 2020.

Davidovits, P., Hu, J. H., Worsnop, D. R., Zahniser, M. S., and Kolb, C. E.: Entry of gas molecules into liquids, Faraday Discuss., 100, 65–81, https://doi.org/10.1039/fd9950000065, 1995.

De Laat, J. and Le, T. G.: Kinetics and modeling of the Fe(III)/H_2O_2 system in the presence of sulfate in acidic aqueous solutions, Environ. Sci. Technol., 39, 1811–1818, 2005.

de Meij, A., Krol, M., Dentener, F., Vignati, E., Cuvelier, C., and Thunis, P.: The sensitivity of aerosol in Europe to two different emission inventories and temporal distribution of emissions, Atmos. Chem. Phys., 6, 4287–4309, https://doi.org/10.5194/acp-6-4287-2006, 2006.

Deguillaume, L., Leriche, M., and Chaumerliac, N.: Impact of radical versus non-radical pathway in the Fenton chemistry on the iron redox cycle in clouds, Chemosphere, 60, 718–724, https://doi.org/10.1016/j.chemosphere.2005.03.052, 2005.

Edwards, J. O. and Mueller., J. J.: The rates of oxidation of nitrite ion by several peroxides, Inorg. Chem., 1, 696–699, 1962.

Elser, M., Huang, R.-J., Wolf, R., Slowik, J. G., Wang, Q., Canonaco, F., Li, G., Bozzetti, C., Daellenbach, K. R., Huang, Y., Zhang, R., Li, Z., Cao, J., Baltensperger, U., El-Haddad, I., and Prévôt, A. S. H.: New insights into $PM_{2.5}$ chemical composition and sources in two major cities in China during extreme haze events using aerosol mass spectrometry, Atmos. Chem. Phys., 16, 3207–3225, https://doi.org/10.5194/acp-16-3207-2016, 2016.

EMEP: Convention on Long-range Transboundary Air Pollution (CLRTAP) programme, EMEP [data set], available at: https://www.emep.int/, last access: 8 August 2020.

Emmons, L. K., Walters, S., Hess, P. G., Lamarque, J.-F., Pfister, G. G., Fillmore, D., Granier, C., Guenther, A., Kinnison, D., Laepple, T., Orlando, J., Tie, X., Tyndall, G., Wiedinmyer,

C., Baughcum, S. L., and Kloster, S.: Description and evaluation of the Model for Ozone and Related chemical Tracers, version 4 (MOZART-4), Geosci. Model Dev., 3, 43–67, https://doi.org/10.5194/gmd-3-43-2010, 2010.

Emmons, L. K., Schwantes, R. H., Orlando, J. J., Tyndall, G., Kinnison, D., Lamarque, J. F., Marsh, D., Mills, M. J., Tilmes, S., Bardeen, C., Buchholz, R. R., Conley, A., Gettelman, A., Garcia, R., Simpson, I., Blake, D. R., Meinardi, S., and Pétron, G.: The Chemistry Mechanism in the Community Earth System Model Version 2 (CESM2), J. Adv. Model. Earth Sy., 12, 1–21, https://doi.org/10.1029/2019ms001882, 2020.

Ervens, B.: Modeling the processing of aerosol and trace gases in clouds and fogs, Chem. Rev., 115, 4157–4198, https://doi.org/10.1021/cr5005887, 2015.

Exner, M.: Bildung und Reaktionen von Radikalen und Radikalanionen in wäßriger Phase, Diploma Thesis, Georg-August-University Göttingen, Göttingen, 1990.

Exner, M., Herrmann, H., and Zellner, R.: Laser-Based Studies of Reactions of the Nitrate Radical in Aqueous-Solution, Ber. Bunsen Phys. Chem., 96, 470–477, https://doi.org/10.1002/bbpc.19920960347, 1992.

Exner, M., Herrmann, H., and Zellner, R.: Rate Constants for the Reactions of the NO_3 Radical with $HCOOH/HCOO^-$ and CH_3COOH/CH_3COO^- in Aqueous-Solution between 278 and 328 K, J. Atmos. Chem., 18, 359–378, https://doi.org/10.1007/Bf00712451, 1994.

Faloona, I.: Sulfur processing in the marine atmospheric boundary layer: A review and critical assessment of modeling uncertainties, Atmos. Environ., 43, 2841–2854, https://doi.org/10.1016/j.atmosenv.2009.02.043, 2009.

Feng, L., Smith, S. J., Braun, C., Crippa, M., Gidden, M. J., Hoesly, R., Klimont, Z., van Marle, M., van den Berg, M., and van der Werf, G. R.: The generation of gridded emissions data for CMIP6, Geosci. Model Dev., 13, 461–482, https://doi.org/10.5194/gmd-13-461-2020, 2020.

Fenton, H. J. H.: LXXIII.—Oxidation of tartaric acid in presence of iron, Journal of the Chemical Society Transactions, 65, 899–910, 1894.

Fischer, M. and Warneck, P.: Photodecomposition and photooxidation of hydrogen sulfite in aqueous solution, J. Phys. Chem.-US, 100, 15111–15117, 1996.

Flemming, J., Huijnen, V., Arteta, J., Bechtold, P., Beljaars, A., Blechschmidt, A.-M., Diamantakis, M., Engelen, R. J., Gaudel, A., Inness, A., Jones, L., Josse, B., Katragkou, E., Marecal, V., Peuch, V.-H., Richter, A., Schultz, M. G., Stein, O., and Tsikerdekis, A.: Tropospheric chemistry in the Integrated Forecasting System of ECMWF, Geosci. Model Dev., 8, 975–1003, https://doi.org/10.5194/gmd-8-975-2015, 2015.

Gankanda, A., Coddens, E. M., Zhang, Y., Cwiertny, D. M., and Grassian, V. H.: Sulfate formation catalyzed by coal fly ash, mineral dust and iron(iii) oxide: variable influence of temperature and light, Environ. Sci. Proc. Imp., 18, 1484–1491, https://doi.org/10.1039/c6em00430j, 2016.

Geng, G., Xiao, Q., Zheng, Y., Tong, D., Zhang, Y., Zhang, X., Zhang, Q., He, K., and Liu, Y.: Impact of China's Air Pollution Prevention and Control Action Plan on $PM_{2.5}$ chemical composition over eastern China, Sci. China Earth Sci., 62, 1872–1884, https://doi.org/10.1007/s11430-018-9353-x, 2019.

George, C., Ponche, J. L., Mirabel, P., Behnke, W., Scheer, V., and Zetzsch, C.: Study of the Uptake of N_2O_5 by Water and NaCl Solutions, J. Phys. Chem.-US, 98, 8780–8784, https://doi.org/10.1021/j100086a031, 1994.

Georgiou, G. K., Christoudias, T., Proestos, Y., Kushta, J., Hadjinicolaou, P., and Lelieveld, J.: Air quality modelling in the summer over the eastern Mediterranean using WRF-Chem: chemistry and aerosol mechanism intercomparison, Atmos. Chem. Phys., 18, 1555–1571, https://doi.org/10.5194/acp-18-1555-2018, 2018.

Goto, D., Nakajima, T., Dai, T., Takemura, T., Kajino, M., Matsui, H., Takami, A., Hatakeyama, S., Sugimoto, N., Shimizu, A., and Ohara, T.: An evaluation of simulated particulate sulfate over East Asia through global model intercomparison, J. Geophys. Res.-Atmos., 120, 6247–6270, https://doi.org/10.1002/2014jd021693, 2015.

Graedel, T. E. and Weschler, C. J.: Chemistry within Aqueous Atmospheric Aerosols and Raindrops, Rev. Geophys., 19, 505–539, https://doi.org/10.1029/RG019i004p00505, 1981.

Guo, H., Weber, R. J., and Nenes, A.: High levels of ammonia do not raise fine particle pH sufficiently to yield nitrogen oxide-dominated sulfate production, Sci. Rep.-UK, 7, 12109, https://doi.org/10.1038/s41598-017-11704-0, 2017.

Guth, J., Josse, B., Marécal, V., Joly, M., and Hamer, P.: First implementation of secondary inorganic aerosols in the MOCAGE version R2.15.0 chemistry transport model, Geosci. Model Dev., 9, 137–160, https://doi.org/10.5194/gmd-9-137-2016, 2016.

Haber, F. and Weiss, J.: The catalytic decomposition of hydrogen peroxide by iron salts, P. R. Soc. London, 147, 332–351, https://doi.org/10.1098/rspa.1934.0221, 1934.

Hanson, D. R., Burkholder, J. B., Howard, C. J., and Ravishankara, A. R.: Measurement of OH and HO_2 Radical Uptake Coefficients on Water and Sulfuric-Acid Surfaces, J. Phys. Chem.-US, 96, 4979–4985, https://doi.org/10.1021/j100191a046, 1992.

Harned, H. S. and Owen, B. B.: The Physical Chemistry of Electrolytic Solutions, 3rd edn., Reinhold, New York.1958.

Harris, E., Sinha, B., van Pinxteren, D., Tilgner, A., Fomba, K. W., Schneider, J., Roth, A., Gnauk, T., Fahlbusch, B., Mertes, S., Lee, T., Collett, J., Foley, S., Borrmann, S., Hoppe, P., and Herrmann, H.: Enhanced Role of Transition Metal Ion Catalysis During In-Cloud Oxidation of SO_2, Science, 340, 727–730, https://doi.org/10.1126/science.1230911, 2013.

He, G. and He, H.: Water Promotes the Oxidation of SO_2 by O_2 over Carbonaceous Aerosols, Environ. Sci. Technol., 54, 7070–7077, https://doi.org/10.1021/acs.est.0c00021, 2020.

He, G., Ma, J., and He, H.: Role of Carbonaceous Aerosols in Catalyzing Sulfate Formation, ACS Catal., 8, 3825–3832, https://doi.org/10.1021/acscatal.7b04195, 2018.

He, H., Wang, Y., Ma, Q., Ma, J., Chu, B., Ji, D., Tang, G., Liu, C., Zhang, H., and Hao, J.: Mineral dust and NO_x promote the conversion of SO_2 to sulfate in heavy pollution days, Sci. Rep.-UK, 4, 4172, https://doi.org/10.1038/srep04172, 2014.

He, J., Zhang, Y., Glotfelty, T., He, R., Bennartz, R., Rausch, J., and Sartelet, K.: Decadal simulation and comprehensive evaluation of CESM/CAM5.1 with advanced chemistry, aerosol microphysics, and aerosol–cloud interactions, J. Adv. Model. Earth Sy., 7, 110–141, https://doi.org/10.1002/2014ms000360, 2015a.

He, J., Zhang, Y., Tilmes, S., Emmons, L., Lamarque, J.-F., Glotfelty, T., Hodzic, A., and Vitt, F.: CESM/CAM5 improvement and application: comparison and evaluation of updated

CB05_GE and MOZART-4 gas-phase mechanisms and associated impacts on global air quality and climate, Geosci. Model Dev., 8, 3999–4025, https://doi.org/10.5194/gmd-8-3999-2015, 2015b.

Heal, M. R., Hibbs, L. R., Agius, R. M., and Beverland, I. J.: Total and water-soluble trace metal content of urban background PM_{10}, $PM_{2.5}$ and black smoke in Edinburgh, UK, Atmos. Environ., 39, 1417–1430, https://doi.org/10.1016/j.atmosenv.2004.11.026, 2005.

Hedegaard, G. B., Brandt, J., Christensen, J. H., Frohn, L. M., Geels, C., Hansen, K. M., and Stendel, M.: Impacts of climate change on air pollution levels in the Northern Hemisphere with special focus on Europe and the Arctic, Atmos. Chem. Phys., 8, 3337–3367, https://doi.org/10.5194/acp-8-3337-2008, 2008.

Herrmann, H. and Zellner, R.: Reactions of NO_3 radicals in aqueous solution, in: N-Centered Radicals John Wiley and Sons Ltd, 1998.

Herrmann, H., Exner, M., and Zellner, R.: Reactivity Trends in Reactions of the Nitrate Radical (NO_3) with Inorganic and Organic Cloudwater Constituents, Geochim. Cosmochim. Ac., 58, 3239–3244, https://doi.org/10.1016/0016-7037(94)90051-5, 1994.

Herrmann, H., Reese, A., and Zellner, R.: Time-Resolved Uv/Vis Diode-Array Absorption-Spectroscopy of SO_x^- ($x = 3$, 4, 5) Radical-Anions in Aqueous-Solution, J Mol Struct, 348, 183–186, https://doi.org/10.1016/0022-2860(95)08619-7, 1995.

Herrmann, H., Jacobi, H. W., Raabe, G., Reese, A., and Zellner, R.: Laser-spectroscopic laboratory studies of atmospheric aqueous phase free radical chemistry, Fresen J Anal Chem, 355, 343–344, 1996.

Herrmann, H., Ervens, B., Jacobi, H. W., Wolke, R., Nowacki, P., and Zellner, R.: CAPRAM2.3: A chemical aqueous phase radical mechanism for tropospheric chemistry, J. Atmos. Chem., 36, 231–284, https://doi.org/10.1023/A:1006318622743, 2000.

Herrmann, H., Schaefer, T., Tilgner, A., Styler, S. A., Weller, C., Teich, M., and Otto, T.: Tropospheric aqueous-phase chemistry: kinetics, mechanisms, and its coupling to a changing gas phase, Chem. Rev., 115, 4259–4334, https://doi.org/10.1021/cr500447k, 2015.

Hoffmann, M. R.: On the Kinetics and Mechanism of Oxidation of Aquated Sulfur–Dioxide by Ozone, Atmos. Environ., 20, 1145–1154, https://doi.org/10.1016/0004-6981(86)90147-2, 1986.

Hoffman, M. R. and Calvert, J. G.: Chemical transformation modules for Eulerian Acid Deposition Models, U.S. Environ. Prot. Agency, Research Triangle Park, N.C., 1985.

Hoigne, J. and Bader, H.: Rate Constants of Reactions of Ozone with Organic and Inorganic-Compounds in Water .2. Dissociating Organic-Compounds, Water Res., 17, 185–194, 1983a.

Hoigne, J. and Bader, H.: Rate Constants of Reactions of Ozone with Organic and Inorganic-Compounds in Water .1. Non-Dissociating Organic-Compounds, Water Res., 17, 173–183, 1983b.

Hong, C., Zhang, Q., Zhang, Y., Tang, Y., Tong, D., and He, K.: Multi-year downscaling application of two-way coupled WRF v3.4 and CMAQ v5.0.2 over east Asia for regional climate and air quality modeling: model evaluation and aerosol direct effects, Geosci. Model Dev., 10, 2447–2470, https://doi.org/10.5194/gmd-10-2447-2017, 2017.

Hsu, S.-C., Liu, S. C., Arimoto, R., Shiah, F.-K., Gong, G.-C., Huang, Y.-T., Kao, S.-J., Chen, J.-P., Lin, F.-J., Lin, C.-Y., Huang, J.-C., Tsai, F., and Lung, S.-C. C.: Effects of acidic processing, transport history, and dust and sea salt loadings on the dissolution of iron from Asian dust, J. Geophys. Res., 115, D19313, https://doi.org/10.1029/2009jd013442, 2010.

Hsu, S.-C., Lin, F.-J., Liu, T.-H., Lin, S.-H., Kao, S.-J., Tseng, C.-M., and Huang, C.-H.: Short time dissolution kinetics of refractory elements Fe, Al, and Ti in Asian outflow-impacted marine aerosols and implications, Atmos. Environ., 79, 93–100, https://doi.org/10.1016/j.atmosenv.2013.06.037, 2013.

Huang, L., An, J., Koo, B., Yarwood, G., Yan, R., Wang, Y., Huang, C., and Li, L.: Sulfate formation during heavy winter haze events and the potential contribution from heterogeneous SO_2 + NO_2 reactions in the Yangtze River Delta region, China, Atmos. Chem. Phys., 19, 14311–14328, https://doi.org/10.5194/acp-19-14311-2019, 2019.

Huang, L. B., Cochran, R. E., Coddens, E. M., and Grassian, V. H.: Formation of Organosulfur Compounds through Transition Metal Ion-Catalyzed Aqueous Phase Reactions, Environ. Sci. Tech. Let., 5, 315–321, https://doi.org/10.1021/acs.estlett.8b00225, 2018.

Huang, X., Song, Y., Zhao, C., Li, M., Zhu, T., Zhang, Q., and Zhang, X.: Pathways of sulfate enhancement by natural and anthropogenic mineral aerosols in China, J. Geophys. Res.-Atmos., 119, 14165–14179, https://doi.org/10.1002/2014jd022301, 2014.

Huie, R. E. and Clifton, C. L.: Temperature-Dependence of the Rate Constants for Reactions of the Sulfate Radical, SO_4^-, with Anions, J. Phys. Chem.-US, 94, 8561–8567, https://doi.org/10.1021/j100386a015, 1990.

Huie, R. E. and Neta, P.: Rate Constants for Some Oxidations of S(IV) by Radicals in Aqueous-Solutions, Atmos. Environ., 21, 1743–1747, 1987.

Huie, R. E., Shoute, L. C. T., and Neta, P.: Temperature-Dependence of the Rate Constants for Reactions of the Carbonate Radical with Organic and Inorganic Reductants, Int. J. Chem. Kinet., 23, 541–552, https://doi.org/10.1002/kin.550230606, 1991.

Hung, H. M., Hsu, M. N., and Hoffmann, M. R.: Quantification of SO_2 Oxidation on Interfacial Surfaces of Acidic Micro-Droplets: Implication for Ambient Sulfate Formation, Environ. Sci. Technol., 52, 9079–9086, https://doi.org/10.1021/acs.est.8b01391, 2018.

Im, U., Christensen, J. H., Geels, C., Hansen, K. M., Brandt, J., Solazzo, E., Alyuz, U., Balzarini, A., Baro, R., Bellasio, R., Bianconi, R., Bieser, J., Colette, A., Curci, G., Farrow, A., Flemming, J., Fraser, A., Jimenez-Guerrero, P., Kitwiroon, N., Liu, P., Nopmongcol, U., Palacios-Peña, L., Pirovano, G., Pozzoli, L., Prank, M., Rose, R., Sokhi, R., Tuccella, P., Unal, A., Vivanco, M. G., Yarwood, G., Hogrefe, C., and Galmarini, S.: Influence of anthropogenic emissions and boundary conditions on multi-model simulations of major air pollutants over Europe and North America in the framework of AQMEII3, Atmos. Chem. Phys., 18, 8929–8952, https://doi.org/10.5194/acp-18-8929-2018, 2018.

Ingall, E., Feng, Y., Longo, A., Lai, B., Shelley, R., Landing, W., Morton, P., Nenes, A., Mihalopoulos, N., Violaki, K., Gao, Y., Sahai, S., and Castorina, E.: Enhanced Iron Solubility at Low pH in Global Aerosols, Atmosphere, 9, 201–207, https://doi.org/10.3390/atmos9050201, 2018.

Itahashi, S.: Toward Synchronous Evaluation of Source Apportionments for Atmospheric Concentration and Deposition of Sulfate

Aerosol Over East Asia, J. Geophys. Res.-Atmos., 123, 2927–2953, https://doi.org/10.1002/2017jd028110, 2018.

Itahashi, S., Yamaji, K., Chatani, S., and Hayami, H.: Refinement of Modeled Aqueous-Phase Sulfate Production via the Fe- and Mn-Catalyzed Oxidation Pathway, Atmosphere, 9, 132–148, https://doi.org/10.3390/atmos9040132, 2018.

Jacob, D. J.: Chemistry of OH in Remote Clouds and Its Role in the Production of Formic-Acid and Peroxymonosulfate, J. Geophys. Res.-Atmos., 91, 9807–9826, https://doi.org/10.1029/JD091iD09p09807, 1986.

Jacob, D. J.: Heterogeneous chemistry and tropospheric ozone, Atmos. Environ., 34, 2131–2159, https://doi.org/10.1016/S1352-2310(99)00462-8, 2000.

Jacobsen, F., Holcman, J., and Sehested, K.: Activation parameters of ferryl ion reactions in aqueous acid solutions, Int. J. Chem. Kinet., 29, 17–24, 1997.

Jacobsen, F., Holcman, J., and Sehested, K.: Reactions of the ferryl ion with some compounds found in cloud water, Int. J. Chem. Kinet., 30, 215–221, 1998.

Jayson, G. G., Parsons, B. J., and Swallow, A. J.: Oxidation of Ferrous Ions by Perhydroxyl Radicals, J. Chem. Soc. Farad. T. 1, 69, 236–242, https://doi.org/10.1039/f19736900236, 1973.

Jo, Y.-J., Lee, H.-J., Jo, H.-Y., Woo, J.-H., Kim, Y., Lee, T., Heo, G., Park, S.-M., Jung, D., Park, J., and Kim, C.-H.: Changes in inorganic aerosol compositions over the Yellow Sea area from impact of Chinese emissions mitigation, Atmos. Res., 240, 1–10, https://doi.org/10.1016/j.atmosres.2020.104948, 2020.

Kajino, M., Deushi, M., Maki, T., Oshima, N., Inomata, Y., Sato, K., Ohizumi, T., and Ueda, H.: Modeling wet deposition and concentration of inorganics over Northeast Asia with MRI-PM/c, Geosci. Model Dev., 5, 1363–1375, https://doi.org/10.5194/gmd-5-1363-2012, 2012.

Kan, H., Chen, R., and Tong, S.: Ambient air pollution, climate change, and population health in China, Environ. Int., 42, 10–19, https://doi.org/10.1016/j.envint.2011.03.003, 2012.

Khan, I. and Brimblecombe, P.: Henry's law constants of low molecular weight (<130) organic acids, J. Aerosol Sci., 23, S897–S900, 1992.

Kirchner, W., Welter, F., Bongartz, A., Kames, J., Schweighoefer, S., and Schurath, U.: Trace Gas-Exchange at the Air-Water-Interface – Measurements of Mass Accommodation Coefficients, J. Atmos. Chem., 10, 427–449, https://doi.org/10.1007/Bf00115784, 1990.

Kläning, U. K., Sehested, K., and Holcman, J.: Standard Gibbs free energy of formation of the hydroxyl radical in aqueous solution: rate constants for the reaction $ClO_2^- + O_3 \rightleftarrows O_3^- + ClO_2$, J. Phys. Chem., 89, 760–763, 1985.

Lakey, P. S., George, I. J., Baeza-Romero, M. T., Whalley, L. K., and Heard, D. E.: Organics Substantially Reduce HO_2 Uptake onto Aerosols Containing Transition Metal ions, J. Phys. Chem. A, 120, 1421–1430, https://doi.org/10.1021/acs.jpca.5b06316, 2016.

Lamarque, J.-F., Emmons, L. K., Hess, P. G., Kinnison, D. E., Tilmes, S., Vitt, F., Heald, C. L., Holland, E. A., Lauritzen, P. H., Neu, J., Orlando, J. J., Rasch, P. J., and Tyndall, G. K.: CAM-chem: description and evaluation of interactive atmospheric chemistry in the Community Earth System Model, Geosci. Model Dev., 5, 369–411, https://doi.org/10.5194/gmd-5-369-2012, 2012.

Lammel, G., Perner, D., and Warneck, P.: Decomposition of Pernitric Acid in Aqueous-Solution, J. Phys. Chem.-US, 94, 6141–6144, https://doi.org/10.1021/j100378a091, 1990.

Lee, Y. N.: Atmospheric aqueous-phase reactions of nitrogen species, in: Gas–Liquid Chemistry of Natural Waters, Brookhaven National Laboratory, Brookhaven, NY, 20/21-20/10, 1984.

Lee, Y. N. and Lind, J. A.: Kinetics of Aqueous-Phase Oxidation of Nitrogen(III) by Hydrogen-Peroxide, J. Geophys. Res.-Atmos., 91, 2793–2800, 1986.

Lee, Y. N. and Schwartz, S. E.: Kinetics of oxidation of aqueous sulfur(IV) by nitrogendioxide, in: Precipitation Scavenging, Dry Deposition and Resuspension, vol. 1, edited by: Pruppacher, H. R., Semonin, R. G., and Slinn, W. G. N., Elsevier, New York, 1983.

Lelieveld, J. and Crutzen, P. J.: The Role of Clouds in Tropospheric Photochemistry, J. Atmos. Chem., 12, 229–267, https://doi.org/10.1007/Bf00048075, 1991.

Lente, G. and Fabian, I.: Kinetics and mechanism of the oxidation of sulfur(IV) by iron(III) at metal ion excess, J. Chem. Soc. Dalton, 778–784, 2002.

Li, G., Bei, N., Cao, J., Huang, R., Wu, J., Feng, T., Wang, Y., Liu, S., Zhang, Q., Tie, X., and Molina, L. T.: A possible pathway for rapid growth of sulfate during haze days in China, Atmos. Chem. Phys., 17, 3301–3316, https://doi.org/10.5194/acp-17-3301-2017, 2017.

Li, J., Chen, X., Wang, Z., Du, H., Yang, W., Sun, Y., Hu, B., Li, J., Wang, W., Wang, T., Fu, P., and Huang, H.: Radiative and heterogeneous chemical effects of aerosols on ozone and inorganic aerosols over East Asia, Sci. Total Environ., 622–623, 1327–1342, https://doi.org/10.1016/j.scitotenv.2017.12.041, 2018.

Li, J., Zhang, Y. L., Cao, F., Zhang, W., Fan, M., Lee, X., and Michalski, G.: Stable Sulfur Isotopes Revealed a Major Role of Transition-Metal Ion-Catalyzed SO_2 Oxidation in Haze Episodes, Environ. Sci. Technol., 54, 2626–2634, https://doi.org/10.1021/acs.est.9b07150, 2020.

Li, L., Hoffmann, M. R., and Colussi, A. J.: Role of Nitrogen Dioxide in the Production of Sulfate during Chinese Haze-Aerosol Episodes, Environ. Sci. Technol., 52, 2686–2693, https://doi.org/10.1021/acs.est.7b05222, 2018.

Liang, J. Y. and Jacobson, M. Z.: A study of sulfur dioxide oxidation pathways over a range of liquid water contents, pH values, and temperatures, J. Geophys. Res.-Atmos., 104, 13749–13769, https://doi.org/10.1029/1999jd900097, 1999.

Lind, J. A. and Kok, G. L.: Correction to 'Henry's law determinations for aqueous solutions of hydrogen peroxide, methylhydroperoxide and peroxyacetic acid', J. Geophys. Res., 99, 21119, https://doi.org/10.1029/94JD01155, 1994.

Lind, J. A., Lazrus, A. L., and Kok, G. L.: Aqueous Phase Oxidation of Sulfur(IV) by Hydrogen-Peroxide, Methylhydroperoxide, and Peroxyacetic Acid, J. Geophys. Res.-Atmos., 92, 4171–4177, https://doi.org/10.1029/JD092iD04p04171, 1987.

Liu, F., Choi, S., Li, C., Fioletov, V. E., McLinden, C. A., Joiner, J., Krotkov, N. A., Bian, H., Janssens-Maenhout, G., Darmenov, A. S., and da Silva, A. M.: A new global anthropogenic SO_2 emission inventory for the last decade: a mosaic of satellite-derived and bottom-up emissions, Atmos. Chem. Phys., 18, 16571–16586, https://doi.org/10.5194/acp-18-16571-2018, 2018.

Liu, J., Horowitz, L. W., Fan, S., Carlton, A. G., and Levy, H.: Global in-cloud production of secondary organic aerosols: Implementation of a detailed chemical mechanism in the GFDL atmospheric model AM3, J. Geophys. Res.-Atmos., 117, D15303, https://doi.org/10.1029/2012jd017838, 2012.

Liu, X., Penner, J. E., Das, B., Bergmann, D., Rodriguez, J. M., Strahan, S., Wang, M., and Feng, Y.: Uncertainties in global aerosol simulations: Assessment using three meteorological data sets, J. Geophys. Res., 112, D11202, https://doi.org/10.1029/2006jd008216, 2007.

Liu, X., Easter, R. C., Ghan, S. J., Zaveri, R., Rasch, P., Shi, X., Lamarque, J.-F., Gettelman, A., Morrison, H., Vitt, F., Conley, A., Park, S., Neale, R., Hannay, C., Ekman, A. M. L., Hess, P., Mahowald, N., Collins, W., Iacono, M. J., Bretherton, C. S., Flanner, M. G., and Mitchell, D.: Toward a minimal representation of aerosols in climate models: description and evaluation in the Community Atmosphere Model CAM5, Geosci. Model Dev., 5, 709–739, https://doi.org/10.5194/gmd-5-709-2012, 2012.

Logager, T., Holcman, J., Sehested, K., and Pedersen, T.: Oxidation of Ferrous-Ions by Ozone in Acidic Solutions, Inorg. Chem., 31, 3523–3529, 1992.

Logager, T., Sehested, K., and Holcman, J.: Rate Constants of the Equilibrium Reactions $SO_4^- + HNO_3 \rightleftarrows HSO_4^- + NO_3$ and $SO_4^- + NO_3^- \rightleftarrows SO_4^{2-} + NO_3$, Radiat. Phys. Chem., 41, 539–543, https://doi.org/10.1016/0969-806x(93)90017-O, 1993.

Ma, J., Chu, B., Liu, J., Liu, Y., Zhang, H., and He, H.: NO_x promotion of SO_2 conversion to sulfate: An important mechanism for the occurrence of heavy haze during winter in Beijing, Environ. Pollut., 233, 662–669, https://doi.org/10.1016/j.envpol.2017.10.103, 2018.

Mao, J., Fan, S., Jacob, D. J., and Travis, K. R.: Radical loss in the atmosphere from Cu-Fe redox coupling in aerosols, Atmos. Chem. Phys., 13, 509–519, https://doi.org/10.5194/acp-13-509-2013, 2013.

Mao, J., Fan, S., and Horowitz, L. W.: Soluble Fe in Aerosols Sustained by Gaseous HO_2 Uptake, Environ. Sci. Tech. Let., 4, 98–104, https://doi.org/10.1021/acs.estlett.7b00017, 2017.

Martin, L. R., Damschen, D. E., and Judeikis, H. S.: Sulfur Dioxide Oxidation Reactions in Aqueous Solution, U.S. Environmental Protection Agency, Research Triangle Park, NC, 1981.

Martin, L. R., Hill, M. W., Tai, A. F., and Good, T. W.: The Iron Catalyzed Oxidation of Sulfur(IV) in Aqueous-Solution – Differing Effects of Organics at High and Low pH, J. Geophys. Res.-Atmos., 96, 3085–3097, 1991.

Maruthamuthu, P. and Neta, P.: Radiolytic Chain Decomposition of Peroxomonophosphoric and Peroxomonosulfuric Acids, J. Phys. Chem.-US, 81, 937–940, 1977.

Maruthamuthu, P. and Neta, P.: Phosphate Radicals – Spectra, Acid-Base Equilibria, and Reactions with Inorganic-Compounds, J. Phys. Chem.-US, 82, 710–713, 1978.

Mathur, R.: Multiscale Air Quality Simulation Platform (MAQSIP): Initial applications and performance for tropospheric ozone and particulate matter, J. Geophys. Res., 110, D13308, https://doi.org/10.1029/2004jd004918, 2005.

Matthijsen, J., Builtjes, P. J. H., and Sedlak, D. L.: Cloud Model Experiments of the Effect of Iron and Copper on Tropospheric Ozone under Marine and Continental Conditions, Meteorol. Atmos. Phys., 57, 43–60, https://doi.org/10.1007/Bf01044153, 1995.

McArdle, J. V. and Hoffmann, M. R.: Kinetics and Mechanism of the Oxidation of Aquated Sulfur-Dioxide by Hydrogen-Peroxide at Low Ph, J. Phys. Chem.-US, 87, 5425–5429, 1983.

McDaniel, M. F. M., Ingall, E. D., Morton, P. L., Castorina, E., Weber, R. J., Shelley, R. U., Landing, W. M., Longo, A. F., Feng, Y., and Lai, B.: Relationship between Atmospheric Aerosol Mineral Surface Area and Iron Solubility, ACS Earth and Space Chemistry, 3, 2443–2451, https://doi.org/10.1021/acsearthspacechem.9b00152, 2019.

McElroy, W. J.: An experimental study of the reactions of some salts of oxy-sulphur acids and reduced sulphur compounds with strong oxidants (O_3, H_2O_2, and HSO_5^-), Cent. Electr. Generating Board, Leatherhead, England, 1987.

McElroy, W. J. and Waygood, S. J.: Kinetics of the Reactions of the SO_4^- Radical with SO_4^-, $S_2O_8^{2-}$, H_2O and Fe^{2+}, J. Chem. Soc. Faraday T., 86, 2557–2564, https://doi.org/10.1039/ft9908602557, 1990.

Miller, C. J., Rose, A. L., and Waite, T. D.: Hydroxyl Radical Production by H_2O_2-Mediated Oxidation of Fe(II) Complexed by Suwannee River Fulvic Acid Under Circumneutral Freshwater Conditions, Environ. Sci. Technol., 47, 829–835, 2013.

Millero, F. J. and Sotolongo, S.: The Oxidation of Fe(II) with H_2O_2 in Seawater, Geochim. Cosmochim. Ac., 53, 1867–1873, 1989.

Mirabel, P.: Investigations of the uptake rate of some atmospheric trace gases, RINOXA Final Report, 1996.

Moch, J. M., Dovrou, E., Mickley, L. J., Keutsch, F. N., Liu, Z., Wang, Y., Dombek, T. L., Kuwata, M., Budisulistiorini, S. H., Yang, L., Decesari, S., Paglione, M., Alexander, B., Shao, J., Munger, J. W., and Jacob, D. J.: Global Importance of Hydroxymethanesulfonate in Ambient Particulate Matter: Implications for Air Quality, J. Geophys. Res.-Atmos., 125, e2020JD032706, https://doi.org/10.1029/2020JD032706, 2020.

Myriokefalitakis, S., Ito, A., Kanakidou, M., Nenes, A., Krol, M. C., Mahowald, N. M., Scanza, R. A., Hamilton, D. S., Johnson, M. S., Meskhidze, N., Kok, J. F., Guieu, C., Baker, A. R., Jickells, T. D., Sarin, M. M., Bikkina, S., Shelley, R., Bowie, A., Perron, M. M. G., and Duce, R. A.: Reviews and syntheses: the GESAMP atmospheric iron deposition model intercomparison study, Biogeosciences, 15, 6659–6684, https://doi.org/10.5194/bg-15-6659-2018, 2018.

Olson, T. M. and Hoffmann, M. R.: Hydroxyalkylsulfonate Formation – Its Role as a S(IV) Reservoir in Atmospheric Water Droplets, Atmos. Environ., 23, 985–997, https://doi.org/10.1016/0004-6981(89)90302-8, 1989.

Pandis, S. N. and Seinfeld, J. H.: Sensitivity Analysis of a Chemical Mechanism for Aqueous-Phase Atmospheric Chemistry, J. Geophys. Res.-Atmos., 94, 1105–1126, 1989.

Pang, S. Y., Jiang, J., and Ma, J.: Oxidation of Sulfoxides and Arsenic(III) in Corrosion of Nanoscale Zero Valent Iron by Oxygen: Evidence against Ferryl Ions (Fe(IV)) as Active Intermediates in Fenton Reaction, Environ. Sci. Technol., 45, 307–312, https://doi.org/10.1021/es102401d, 2011.

Park, J. Y. and Lee, Y. N.: Solubility and Decomposition Kinetics of Nitrous-Acid in Aqueous-Solution, J. Phys. Chem.-US, 92, 6294–6302, https://doi.org/10.1021/j100333a025, 1988.

Pikaev, A. K., Sibirska.Gk, Shirshov, E. M., Glazunov, P. Y., and Spitsyn, V. I.: Pulse-Radiolysis of Concentrated Aqueous-Solutions of Nitric-Acid, Dokl. Akad. Nauk. SSSR+, 215, 645–648, 1974.

Pöschl, U. and Shiraiwa, M.: Multiphase chemistry at the atmosphere-biosphere interface influencing climate and public health in the anthropocene, Chem. Rev., 115, 4440–4475, https://doi.org/10.1021/cr500487s, 2015.

Pozzer, A., de Meij, A., Pringle, K. J., Tost, H., Doering, U. M., van Aardenne, J., and Lelieveld, J.: Distributions and regional budgets of aerosols and their precursors simulated with the EMAC chemistry-climate model, Atmos. Chem. Phys., 12, 961–987, https://doi.org/10.5194/acp-12-961-2012, 2012.

Quan, J., Liu, Q., Li, X., Gao, Y., Jia, X., Sheng, J., and Liu, Y.: Effect of heterogeneous aqueous reactions on the secondary formation of inorganic aerosols during haze events, Atmos. Environ., 122, 306–312, https://doi.org/10.1016/j.atmosenv.2015.09.068, 2015.

Raabe, G.: Eine laserphotolytische Studie zur Kinetik der Reaktionen des NO_3-Radikals in wäßriger Lösung, Cuvillier, Göttingen, Germany, 1996.

Redlich, O.: The Dissociation of Strong Electrolytes, Chem. Rev., 39, 333–356, https://doi.org/10.1021/cr60123a005, 1946.

Reese, A., Herrmann, H., and Zellner, R.: Kinetics and spectroscopy of organic peroxyl radicals (RO_2) in aqueous solution, in: Proceedings of Eurotrac Symposium '96 – Transport and Transformation of Pollutants in the Troposphere, 25–29 March 1996, Garmisch Partenkirchen, Germany, 1, 377–381, Accession Number WOS:A1997BH53U00067, 1997.

Rettich, T. R.: Some photochemical reactions of aqueous nitric acid, Diss. Abstr. Int. B, 38, 5968, 1978.

Rudich, Y., Talukdar, R. K., Ravishankara, A. R., and Fox, R. W.: Reactive uptake of NO_3 on pure water and ionic solutions, J. Geophys. Res.-Atmos., 101, 21023–21031, https://doi.org/10.1029/96jd01844, 1996.

Rush, J. D. and Bielski, B. H. J.: Pulse Radiolytic Studies of the Reactions of HO_2/O_2^- with Fe(II)/Fe(III) Ions – the Reactivity of HO_2/O_2^- with Ferric Ions and Its Implication on the Occurrence of the Haber-Weiss Reaction, J. Phys. Chem.-US, 89, 5062–5066, https://doi.org/10.1021/j100269a035, 1985.

Sander, R.: Compilation of Henry's law constants for inorganic and organic species of potential importance in environmental chemistry, Max-Planck Institute of Chemistry, Mainz, Germany, 3, https://doi.org/10.1016/j.ecss.2012.02.006, 1999.

Santana-Casiano, J. M., Gonzaalez-Davila, M., and Millero, F. J.: Oxidation of nanomolar levels of Fe(II) with oxygen in natural waters, Environ. Sci. Technol., 39, 2073–2079, 2005.

Schmidt, K. H.: Electrical conductivity techniques for studying the kinetics of radiation induced chemical reactions in aqueous solutions, Int. J. Radiat. Phys. Ch., 4, 439–468, 1972.

Sedwick, P. N., Sholkovitz, E. R., and Church, T. M.: Impact of anthropogenic combustion emissions on the fractional solubility of aerosol iron: Evidence from the Sargasso Sea, Geochem. Geophy. Geosy., 8, 1–21, https://doi.org/10.1029/2007gc001586, 2007.

Sehested, K., Rasmussen, O. L., and Fricke, H.: Rate Constants of OH with HO_2, O_2^- and $H_2O_2^+$ from Hydrogen Peroxide Formation in Pulse-Irradiated Oxygenated Water, J. Phys. Chem.-US, 72, 626–631, 1968.

Sehested, K., Holcman, J., and Hart, E. J.: Rate Constants and Products of the Reactions of e_{aq}^-, O_2^-, and H with Ozone in Aqueous-Solutions, J. Phys. Chem.-US, 87, 1951–1954, 1983.

Seinfeld, J. H. and Pandis, S. N.: Atmospheric chemistry and physics: from air pollution to climate change, John Wiley & Sons, Inc., Hoboken, New Jersey, USA, 2016.

Sha, T., Ma, X., Jia, H., Tian, R., Chang, Y., Cao, F., and Zhang, Y.: Aerosol chemical component: Simulations with WRF-Chem and comparison with observations in Nanjing, Atmos. Environ., 218, 1–12, https://doi.org/10.1016/j.atmosenv.2019.116982, 2019.

Shao, J., Chen, Q., Wang, Y., Lu, X., He, P., Sun, Y., Shah, V., Martin, R. V., Philip, S., Song, S., Zhao, Y., Xie, Z., Zhang, L., and Alexander, B.: Heterogeneous sulfate aerosol formation mechanisms during wintertime Chinese haze events: air quality model assessment using observations of sulfate oxygen isotopes in Beijing, Atmos. Chem. Phys., 19, 6107–6123, https://doi.org/10.5194/acp-19-6107-2019, 2019.

Shelley, R. U., Landing, W. M., Ussher, S. J., Planquette, H., and Sarthou, G.: Regional trends in the fractional solubility of Fe and other metals from North Atlantic aerosols (GEOTRACES cruises GA01 and GA03) following a two-stage leach, Biogeosciences, 15, 2271–2288, https://doi.org/10.5194/bg-15-2271-2018, 2018.

Shi, G., Xu, J., Shi, X., Liu, B., Bi, X., Xiao, Z., Chen, K., Wen, J., Dong, S., Tian, Y., Feng, Y., Yu, H., Song, S., Zhao, Q., Gao, J., and Russell, A. G.: Aerosol pH Dynamics During Haze Periods in an Urban Environment in China: Use of Detailed, Hourly, Speciated Observations to Study the Role of Ammonia Availability and Secondary Aerosol Formation and Urban Environment, J. Geophys. Res.-Atmos., 124, 9730–9742, https://doi.org/10.1029/2018jd029976, 2019.

Shi, J., Guan, Y., Ito, A., Gao, H., Yao, X., Baker, A. R., and Zhang, D.: High Production of Soluble Iron Promoted by Aerosol Acidification in Fog, Geophys. Res. Lett., 47, 1–8, https://doi.org/10.1029/2019gl086124, 2020.

Sholkovitz, E. R., Sedwick, P. N., and Church, T. M.: Influence of anthropogenic combustion emissions on the deposition of soluble aerosol iron to the ocean: Empirical estimates for island sites in the North Atlantic, Geochim. Cosmochim. Ac., 73, 3981–4003, https://doi.org/10.1016/j.gca.2009.04.029, 2009.

Song, S., Ma, T., Zhang, Y., Shen, L., Liu, P., Li, K., Zhai, S., Zheng, H., Gao, M., Moch, J. M., Duan, F., He, K., and McElroy, M. B.: Global modeling of heterogeneous hydroxymethanesulfonate chemistry, Atmos. Chem. Phys., 21, 457–481, https://doi.org/10.5194/acp-21-457-2021, 2021.

Staehelin, J. and Hoigne, J.: Decomposition of Ozone in Water – Rate of Initiation by Hydroxide Ions and Hydrogen-Peroxide, Environ. Sci. Technol., 16, 676–681, 1982.

Strehlow, H. and Wagner, I.: Flash-Photolysis in Aqueous Nitrite Solutions, Z. Phys. Chem. Neue Fol., 132, 151–160, 1982.

Tan, J., Duan, J., Zhen, N., He, K., and Hao, J.: Chemical characteristics and source of size-fractionated atmospheric particle in haze episode in Beijing, Atmos. Res., 167, 24–33, https://doi.org/10.1016/j.atmosres.2015.06.015, 2016.

Tan, Y., Perri, M. J., Seitzinger, S. P., and Turpin, B. J.: Effects of Precursor Concentration and Acidic Sulfate in Aqueous Glyoxal-OH Radical Oxidation and Implications for Secondary Organic Aerosol, Environ. Sci. Technol., 43, 8105–8112, 2009.

Tang, M., Cziczo, D. J., and Grassian, V. H.: Interactions of Water with Mineral Dust Aerosol: Water Adsorption, Hygroscopicity, Cloud Condensation, and Ice Nucleation, Chem. Rev., 116, 4205–4259, https://doi.org/10.1021/acs.chemrev.5b00529, 2016.

Tang, Y., Thorn, R. P., Mauldin, R. L., and Wine, P. H.: Kinetics and Spectroscopy of the SO_4^- Radical in Aqueous-Solution, J. Photoch. Photobio. A, 44, 243–258, https://doi.org/10.1016/1010-6030(88)80097-2, 1988.

Tao, J., Zhang, L., Cao, J., and Zhang, R.: A review of current knowledge concerning $PM_{2.}5$ chemical composition, aerosol optical properties and their relationships across China, Atmos. Chem. Phys., 17, 9485–9518, https://doi.org/10.5194/acp-17-9485-2017, 2017.

Thomas, J. K.: The rate constants for H atom reactions in aqueous solution, J. Phys. Chem., 67, 2593–2595, 1963.

Tilgner, A., Bräuer, P., Wolke, R., and Herrmann, H.: Modelling multiphase chemistry in deliquescent aerosols and clouds using CAPRAM3.0i, J. Atmos. Chem., 70, 221–256, https://doi.org/10.1007/s10874-013-9267-4, 2013.

Tong, H., Lakey, P. S. J., Arangio, A. M., Socorro, J., Kampf, C. J., Berkemeier, T., Brune, W. H., Poschl, U., and Shiraiwa, M.: Reactive oxygen species formed in aqueous mixtures of secondary organic aerosols and mineral dust influencing cloud chemistry and public health in the Anthropocene, Faraday Discuss., 200, 251–270, https://doi.org/10.1039/c7fd00023e, 2017.

Treinin, A. and Hayon, E.: Absorption Spectra and Reaction Kinetics of NO_2, N_2O_3, and N_2O_4 in Aqueous Solution, J. Am. Chem. Soc., 92, 5821–5828, 1970.

United States Environmental Protection Agency: Pre-Generated Data Files, US EPA [data set], available at: https://aqs.epa.gov/aqsweb/airdata/download_files.html, last access: 19 July 2020.

Wagner, I., Strehlow, H., and Busse, G.: Flash-Photolysis of Nitrate Ions in Aqueous-Solution, Z. Phys. Chem. Neue Fol., 123, 1–33, https://doi.org/10.1524/zpch.1980.123.1.001, 1980.

Walling, C. and Goosen, A.: Mechanism of Ferric Ion Catalyzed Decomposition of Hydrogen-Peroxide – Effect of Organic Substrates, J. Am. Chem. Soc., 95, 2987–2991, https://doi.org/10.1021/ja00790a042, 1973.

Wang, J., Li, J., Ye, J., Zhao, J., Wu, Y., Hu, J., Liu, D., Nie, D., Shen, F., Huang, X., Huang, D. D., Ji, D., Sun, X., Xu, W., Guo, J., Song, S., Qin, Y., Liu, P., Turner, J. R., Lee, H. C., Hwang, S., Liao, H., Martin, S. T., Zhang, Q., Chen, M., Sun, Y., Ge, X., and Jacob, D. J.: Fast sulfate formation from oxidation of SO_2 by NO_2 and HONO observed in Beijing haze, Nat. Commun., 11, 2844, https://doi.org/10.1038/s41467-020-16683-x, 2020.

Wang, R., Balkanski, Y., Boucher, O., Bopp, L., Chappell, A., Ciais, P., Hauglustaine, D., Peñuelas, J., and Tao, S.: Sources, transport and deposition of iron in the global atmosphere, Atmos. Chem. Phys., 15, 6247–6270, https://doi.org/10.5194/acp-15-6247-2015, 2015.

Warneck, P.: The oxidation of sulfur(IV) by reaction with iron(III): a critical review and data analysis, Phys. Chem. Chem. Phys., 20, 4020–4037, https://doi.org/10.1039/c7cp07584g, 2018.

Warneck, P. and Wurzinger, C.: Product Quantum Yields for the 305 nm Photodecomposition of NO_3^- in Aqueous-Solution, J. Phys. Chem.-US, 92, 6278–6283, https://doi.org/10.1021/j100333a022, 1988.

Wei, Y., Chen, X., Chen, H., Li, J., Wang, Z., Yang, W., Ge, B., Du, H., Hao, J., Wang, W., Li, J., Sun, Y., and Huang, H.: IAP-AACM v1.0: a global to regional evaluation of the atmospheric chemistry model in CAS-ESM, Atmos. Chem. Phys., 19, 8269–8296, https://doi.org/10.5194/acp-19-8269-2019, 2019.

Weinsteinlloyd, J. and Schwartz, S. E.: Low-Intensity Radiolysis Study of Free-Radical Reactions in Cloudwater – H_2O_2 Production and Destruction, Environ. Sci. Technol., 25, 791–800, https://doi.org/10.1021/es00016a027, 1991.

Welch, M. J., Lifton, J. F., and Seck, J. A.: Tracer Studies with Radioactive Oxygen-15. Exchange between Carbon Dioxide and Water, J. Phys. Chem.-US, 73, 3351–3356, https://doi.org/10.1021/j100844a033, 1969.

Wiegand, H. L., Orths, C. T., Kerpen, K., Lutze, H. V., and Schmidt, T. C.: Investigation of the Iron-Peroxo Complex in the Fenton Reaction: Kinetic Indication, Decay Kinetics, and Hydroxyl Radical Yields, Environ. Sci. Technol., 51, 14321–14329, https://doi.org/10.1021/acs.est.7b03706, 2017.

Wine, P. H., Tang, Y., Thorn, R. P., Wells, J. R., and Davis, D. D.: Kinetics of Aqueous Phase Reactions of the SO_4^- Radical with Potential Importance in Cloud Chemistry, J. Geophys. Res.-Atmos., 94, 1085–1094, https://doi.org/10.1029/JD094iD01p01085, 1989.

Xie, X., Liu, X., Wang, H., and Wang, Z.: Effects of Aerosols on Radiative Forcing and Climate Over East Asia With Different SO_2 Emissions, Atmosphere, 7, 1–12, https://doi.org/10.3390/atmos7080099, 2016.

Xue, J., Yuan, Z., Griffith, S. M., Yu, X., Lau, A. K., and Yu, J. Z.: Sulfate Formation Enhanced by a Cocktail of High NO_x, SO_2, Particulate Matter, and Droplet pH during Haze-Fog Events in Megacities in China: An Observation-Based Modeling Investigation, Environ. Sci. Technol., 50, 7325–7334, https://doi.org/10.1021/acs.est.6b00768, 2016.

Zellner, R., Exner, M., and Herrmann, H.: Absolute OH quantum yields in the laser photolysis of nitrate, nitrite and dissolved H_2O_2 at 308 and 351 nm in the temperature range 278–353 K, J. Atmos. Chem., 10, 411–425, 1990.

Zellner, R., Herrmann, H., Exner, M., Jacobi, H.-W., Raabe, G., and Reese, A.: Formation and Reactions of Oxidants in the Aqueous Phase, in: Heterogeneous and Liquid Phase Processes, edited by: Warneck, P., Springer, Berlin, p. 146152, 1996.

Zhang, H., Li, J., Ying, Q., Yu, J. Z., Wu, D., Cheng, Y., He, K., and Jiang, J.: Source apportionment of $PM_{2.5}$ nitrate and sulfate in China using a source-oriented chemical transport model, Atmos. Environ., 62, 228–242, https://doi.org/10.1016/j.atmosenv.2012.08.014, 2012.

Zhang, M., Liu, X., Diao, M., D'Alessandro, J. J., Wang, Y., Wu, C., Zhang, D., Wang, Z., and Xie, S.: Impacts of Representing Heterogeneous Distribution of Cloud Liquid and Ice on Phase Partitioning of Arctic Mixed-Phase Clouds with NCAR CAM5, J. Geophys. Res.-Atmos., 124, 13071–13090, https://doi.org/10.1029/2019jd030502, 2019.

Zheng, B., Zhang, Q., Zhang, Y., He, K. B., Wang, K., Zheng, G. J., Duan, F. K., Ma, Y. L., and Kimoto, T.: Heterogeneous chemistry: a mechanism missing in current models to explain secondary inorganic aerosol formation during the January 2013 haze episode in North China, Atmos. Chem. Phys., 15, 2031–2049, https://doi.org/10.5194/acp-15-2031-2015, 2015.

Zheng, H., Song, S., Sarwar, G., Gen, M., Wang, S., Ding, D., Chang, X., Zhang, S., Xing, J., Sun, Y., Ji, D., Chan, C. K., Gao, J., and McElroy, M. B.: Contribution of Particulate Nitrate Photolysis to Heterogeneous Sulfate Formation for Winter Haze in China, Environ. Sci. Technol. Let., 7, 632–638, https://doi.org/10.1021/acs.estlett.0c00368, 2020.

Ziajka, J., Beer, F., and Warneck, P.: Iron-Catalyzed Oxidation of Bisulfite Aqueous-Solution – Evidence for a Free-Radical Chain Mechanism, Atmos. Environ., 28, 2549–2552, https://doi.org/10.1016/1352-2310(94)90405-7, 1994.